RESEARCH ARTICLE

High-temperature emplacement of the Cerro Galán and Toconquis Group ignimbrites (Puna plateau, NW Argentina) determined by TRM analyses

Chiara Lesti · Massimiliano Porreca · Guido Giordano · Massimo Mattei · Raymond A. F. Cas · Heather M. N. Wright · Chris B. Folkes · Josè Viramonte

Abstract Estimates of pyroclastic flow emplacement temperatures in the Cerro Galán ignimbrite and Toconquis Group ignimbrites were determined using thermal remanent magnetization of lithic clasts embedded within the deposits. These ignimbrites belong to the Cerro Galán volcanic system, one of the largest calderas in the world, in the Puna plateau, NW Argentina. Temperature estimates for the 2.08-Ma Cerro Galán ignimbrite are retrieved from 40 sites in 14 localities (176 measured clasts), distributed at different distances from the caldera

and different stratigraphic heights. Additionally, temperature estimates were obtained from 27 sample sites (125 measured clasts) from seven ignimbrite units forming the older Toconquis Group (5.60–4.51 Ma), mainly outcropping along a type section at Rio Las Pitas, Vega Real Grande. The paleomagnetic data obtained by progressive thermal demagnetization show that the clasts of the Cerro Galán ignimbrite have one single magnetic component, oriented close to the expected geomagnetic field at the time of emplacement. Results show therefore that most of the clasts acquired a new magnetization oriented parallel to the magnetic field at the moment of the ignimbrite deposition, suggesting that the clasts were heated up to or above the highest blocking temperature (T_b) of the magnetic minerals ($T_b=580°C$ for magnetite; $T_b=600–630°C$ for hematite). We obtained similar emplacement temperature estimations for six out of the seven volcanic units belonging to the Toconquis Group, with the exception of one unit (Lower Merihuaca), where we found two distinct magnetic components. The estimation of emplacement temperatures in this latter case is constrained at 580–610°C, which are lower than the other ignimbrites. These estimations are also in agreement with the lowest pre-eruptive magma temperatures calculated for the same unit (i.e., 790°C; hornblende–plagioclase thermometer; Folkes et al. 2011b). We conclude that the Cerro Galán ignimbrite and Toconquis Group ignimbrites were emplaced at temperatures equal to or higher than 620°C, except for Lower Merihuaca unit emplaced at lower temperatures. The homogeneity of high temperatures from proximal to distal facies in the Cerro Galán ignimbrite provides constraints for the emplacement model, marked by a relatively low eruption column, low levels of turbulence, air entrainment, surface–water interaction, and a high level of topographic confinement, all ensuring minimal heat loss.

C. Lesti (✉) · M. Porreca · G. Giordano · M. Mattei
Università Roma Tre,
L.go San Leonardo Murialdo,
1 00146 Rome, Italy
e-mail: clesti@uniroma3.it

M. Porreca
Centro de Vulcanologia e Avaliação de Riscos Geológicos (CVARG), Departamento de Geociências,
Universidade dos Açores,
Complexo Científico, 2° Piso,
9500-801 Ponta Delgada, Portugal

R. A. F. Cas · H. M. N. Wright · C. B. Folkes
School of Geosciences, Monash University,
Clayton, VIC 3800, Australia

J. Viramonte
Instituto GEONORTE and CONICET,
Universidad Nacional de Salta,
Buenos Aires 177,
4400 Salta, Argentina

Introduction

Large-scale explosive eruptions, characterized by volcanic explosivity index VEI >7, are the most dangerous eruptions, capable of producing very large volume pyroclastic flows that rapidly travel to great distances from the eruptive center. These eruptions have not been witnessed in historical times and are, therefore, relatively poorly understood. To better understand the emplacement dynamics of these flows, we must either extrapolate from historic observations of small to moderate volume pyroclastic flows, with volumes <10 km³ (Mason et al. 2004), or use indirect measurement techniques and models.

Determination of emplacement temperature provides a strong constraint on interpretation of the transport and depositional system of pyroclastic flows (McClelland et al. 2004). The emplacement temperature of a pyroclastic flow is related to a complex combination of factors such as the initial magmatic temperature, transport path through the atmosphere (including whether the eruption column is buoyant, or boiling over), adiabatic decompression, and heat loss from the flow during lateral transport, due to the interaction of the flow with air and water (e.g., Cas and Wright 1987; Branney and Kokelaar 2002). Conditions at the vent and along flow, such as mass flux and velocity, influence the capability of the flow to entrain air, which in turn, together with the grain size distribution, control the runout distance (Bursik and Woods 1996). The physical parameters on which mobility depends are still debated, but air entrainment (and consequently temperature) is certainly a good candidate, together with eruption rate, grain size distribution, hill slope, and topographic confinement (Bursik and Woods 1996). The temperature of emplacement of pyroclastic flow deposits therefore represents one of the most important measurable physical parameters, as it can be related to the pyroclastic flow mobility, with important implications for hazard assessment.

Paleomagnetic methods provide reliable tools for determining emplacement temperature in ancient ignimbrites (McClelland et al. 2004). Many studies have applied paleomagnetic methodology, beginning with the pioneering study of Aramaki and Akimoto (1957), who used thermal remanent magnetization (TRM) on the bulk ignimbrite deposit to estimate the emplacement temperature. The same technique was then extended to lithic clasts incorporated into ignimbrites (Wright 1978; Hoblitt and Kellogg 1979; Kent et al. 1981; McClelland and Druitt 1989; Bardot 2000;

McClelland et al. 2004; Porreca et al. 2008; Sulpizio et al. 2008) and to pumice clasts (McClelland et al. 2004).

Using thermal demagnetization of lithic clasts, emplacement temperatures have been estimated for several well-known small to large volume ignimbrites, including the 79 A.D. eruption of Vesuvius (180–380°C, 7 km from the vent, Cioni et al. 2004; 140–300°C within and around Pompeii, Zanella et al. 2007), the 1630 BC eruption of Santorini (200–≥580°C McClelland and Druitt 1989; 400–≥580°C 11 km far from vent, Bardot 2000), the 1883 A.D. eruption of Krakatau (475–550°C, subaqueous pyroclastic flow 8 km from the vent; Mandeville et al. 1994), and the 1.8-ka eruption of Taupo (150–≥580°C at more than 40 km from vent, McClelland et al. 2004). The lowest reported emplacement temperatures of pyroclastic density currents are interpreted to have resulted from interaction with external water (<100°C, McClelland et al. 2004; <140°C, Porreca et al. 2006), air (Cioni et al. 2004), and urban structures (Gurioli et al. 2005; Zanella et al. 2007).

Temperature estimates along the flow path provide additional information about the degree and extent of heat loss along the flow and the extent of flow interaction with external media (water and air). McClelland et al. (2004) estimated equilibrium emplacement temperatures at 400–500°C for the 1.8-ka Taupo eruption (bulk volume 30 km³), up to 50 km from the source. In contrast, in proximal facies less than 30 km from the source, the emplacement temperature was evaluated to be between 150°C and 300°C. This variation was interpreted, in combination with field evidence, as being due to interaction of early, proximal flows with lake water that occupied the old caldera depression. Nonetheless, from direct measurements of 1980 Mount St. Helens activity, Banks and Hoblitt (1981) found that the ash cloud temperature dropped initially, while in the ash column, but temperature was largely maintained in the pyroclastic flow. They found an initial drop in temperature of 100°C, from a magmatic temperature of 950°C (Banks and Hoblitt 1981, and references therein) during the first air interaction phase in the convecting column, and a second drop to about 700°C in the first hundreds of meters from the vent. The temperature of the pyroclastic flow then remained constant up to 8 km from the source.

Furthermore, the temperature of the pyroclastic flow at the moment of deposition has also strong influences on post-emplacement processes, such as welding. The glassy material, once deposited, may still show ductile behavior that can develop, along a steep topography, features consistent with rheomorphic flows. The welding process occurs through sintering, compaction, and flattening of the pyroclasts, depending on various parameters, which are still

in debate. Compositional changes, load of the overlying material, volatile content, grain size population, and lithic content are all factors that variably determine the occurrence of welding (e.g., Freundt 1998; Branney and Kokelaar 2002). Quane and Russel (2005) ranked welding intensity in six ranks (I–VI), defined by discrete ranges in physical properties (including porosity, density, point load strength, uniaxial compressive strength, pumice lapilli oblateness, and microfabric orientation) and macroscopic and microscopic textural characteristics. Petrographic characteristics vary from the unconsolidated, incoherent ash matrix, with randomly oriented pumice lapilli lacking any deformation of rank I to the obsidian-like vitrophyre with eutaxitic texture and obsidian-like *fiamme* of rank VI. Welding structures, being related to ductile behavior of glassy shards, are strongly dependent on glass transition temperature of the materials and therefore are particularly useful in defining upper-boundary temperature limit for non-welded deposits.

In this study, we determine the emplacement temperature of the Cerro Galán ignimbrite (CGI) and other older ignimbrites belonging to the Toconquis Group by means of paleomagnetic techniques applied on accessory and/or accidental lithic clasts embedded within the deposits. The thermal structure of these deposits, from proximal to distal locations and at different stratigraphic heights, has been studied in order to constrain the transport and emplacement mechanisms and to define the extent of interaction with external "cooling" factors such as the atmosphere, ground water, surface water, and ground surface in an arid environment. We use paleomagnetic temperature analyses of ignimbrites in the Cerro Galán volcanic system to better understand emplacement conditions and transport dynamics in very large volume pyroclastic flows.

Geological setting and sedimentological features of the Cerro Galán ignimbrites

The Cerro Galán caldera is one of the largest calderas in the world, with a 35×20-km N–S elongated structure, located in the southern margin of the Puna plateau in NW Argentina and ~200 km south of the extensive Altiplano–Puna Volcanic complex (Fig. 1). The caldera
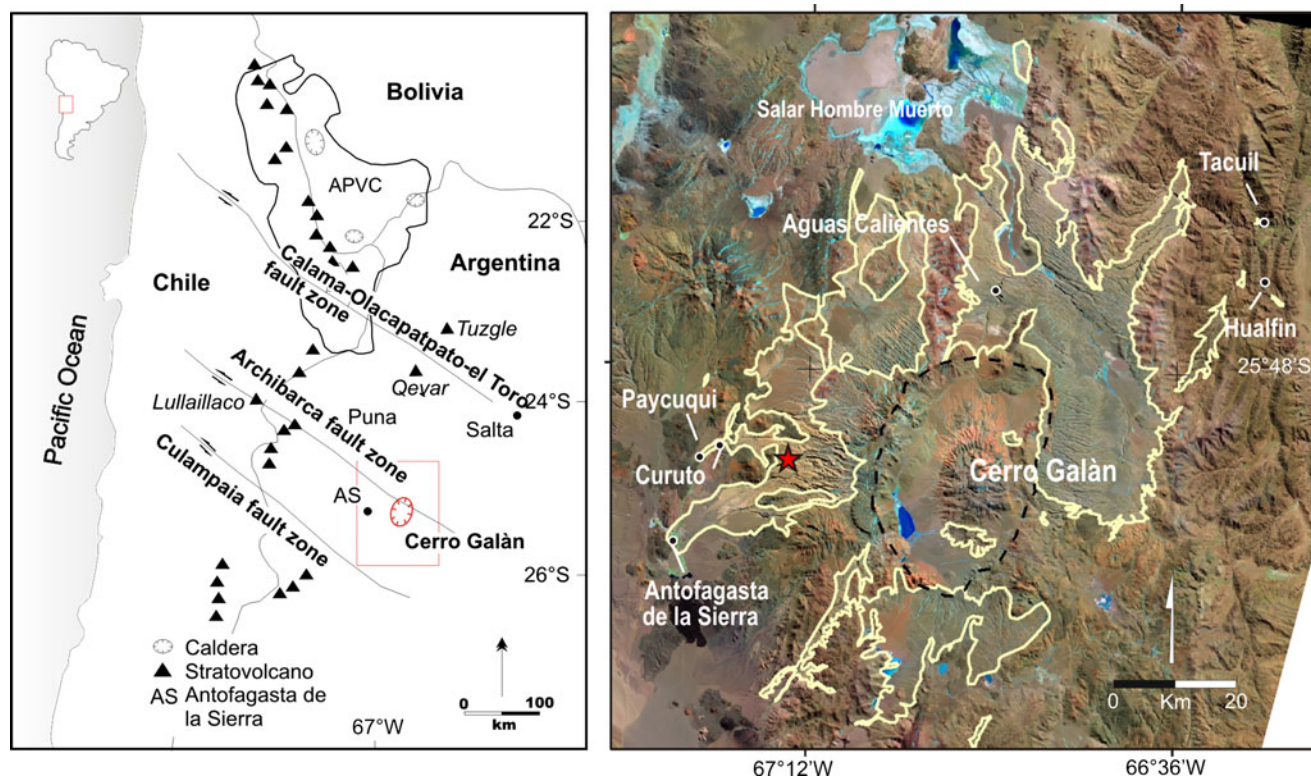
Fig. 1 Location of Cerro Galán caldera in the Puna plateau, northwestern Argentina. **a** Main structural features of central Andes (modified after Riller et al. 2001). *APVC* Altiplano Puna Volcanic Complex; **b** Cerro Galán area (enlargement of *red square* in **a**). Color composition of Landsat ETM+ (bands 7, 4, 2). The Cerro Galán ignimbrite is contoured in *light brown*; the *black solid lines* represent the inferred caldera collapse faults (Folkes et al. 2011a); the *dashed line* follows the topographic caldera rim. *Red star*: location of Fig. 2a section

lies on a N–S trending graben fault zone, the Diablillos–Galán Fault Zone (Coira et al. 1993, Kay et al. 2008), at the intersection with a major NW trending regional Archibarca lineament (Viramonte et al. 1984; Salfity 1984). The caldera is characterized by a large central resurgent dome that exposes the uplifted intracaldera Cerro Galán ignimbrite and several post-ignimbrite lava domes (Sparks et al. 1985).

Francis et al. (1983) and Sparks et al. (1985) recognized that the CGI formed the present caldera and represents the most voluminous eruption of the Cerro Galán volcanic system, with the most distal outcrop at ~74 km north of the current topographic margin. The older ignimbrite deposits, grouped under the name of Toconquis Group, were likely related to an older caldera (Folkes et al. 2011a) and have a smaller, though more poorly constrained volume than the Cerro Galán ignimbrite.

The regional stratigraphy, described in early works by Francis et al. (1983) and Sparks et al. (1985), was recently revised (see Folkes et al. 2011a) and is summarized in Table 1. Nine distinct outflow ignimbrites are recognized, including two newly identified ignimbrite units in the Toconquis Group (Pitas and Vega ignimbrites).

Early ignimbrites of the Toconquis Group are underlain by fall deposits, whereas the Cerro Galán ignimbrite is not. The seven ignimbrites belonging to the Toconquis Group (biotite ^{40}Ar/^{39}Ar age of 5.60–4.51 Ma; Folkes et al. 2011a) are best exposed in a 200-m section at Rio Las Pitas locality, Vega Real Grande section (Fig. 2a). They are largely massive and chaotic, ash matrix supported, crystal rich (up to 50 vol.%), and generally lithic poor (<5 vol.%), except for the Vega ignimbrites with 25% lithics. All the ignimbrites are pumice rich (20–40%), and the Pitas and Real Grande ignimbrites contain pumice concentration zones with individual pumice clasts up to 1 m in diameter.

Table 1 Cerro Galán system stratigraphy and ^{40}Ar/^{39}Ar ages

|	Ignimbrite	Age (Ma)
	Cerro Galàn	2.08+-0.02
		Quiescence Period 1.69 Ma
	Cueva Negra	3.77+-0.08
		Quiescence Period 0.74 Ma
Toconquis Group	Vega	4.51+-0.11
	Real Grande	4.68+-0.07
	Pitas	4.84+-0.04
		Quiescence Period 0.65 Ma
	UpperMerihuaca	5.49+-0.11
	MiddleMerihuaca	5.56+-0.15
	LowerMerihuaca	5.60+-0.20
	Blanco	/

The CGI eruption age is an average of sanidine ^{40}Ar/^{39}Ar ages from samples to the north and west of the caldera by Kay et al. (2011), while for the other units we refer to the biotite ^{40}Ar/^{39}Ar ages by Folkes et al. (2011a)

All the Toconquis Group ignimbrites lack welding textures. The currently preserved areal extent of the Toconquis Group ignimbrites is about 420 km^2, with a total volume of 651 km^3 (DRE). The highly welded Cueva Negra unit (biotite ^{40}Ar/^{39}Ar age of 3.77±0.08 Ma; Folkes et al. 2011a), outcropping on the eastern flanks of the caldera, is not investigated in this study.

The Cerro Galán ignimbrite is the most recent and voluminous ignimbrite (630 km^3 DRE), erupted at 2.08± 0.02 Ma (sanidine ^{40}Ar/^{39}Ar age; Kay et al. 2011) from the Cerro Galán caldera. The CGI outflow sheet extends to 35 km in all directions from the present caldera, with a maximum runout distance of 74 km to the north of the current topographic margin, where the deposit is 15 m thick (Gonzalez 1984). The CGI covers a preserved areal extent of 2,400 km^2. Although rarely visible, the relationship with the underlying topography is valley ponding (Fig. 2b). Vapor-phase alteration and columnar jointing are common, especially where the ignimbrites are confined in paleovalleys (see Wright et al. 2011b and Fig. 2c). No veneer facies have been described associated with the CGI (Cas et al. 2011). The ignimbrite is rhyodacitic in composition, largely characterized by massive facies and up to 200 m thick; it is extremely crystal rich (35–45% of matrix volume), pumice poor (<10%), and lithic poor (<5%) (Fig. 2d, e).

Petrographic analyses show an up-sequence decrease in crystal content in the most recent ignimbrites (vesicle-free; from 55% to 45%), a decrease in amphibole and possibly biotite (Folkes et al. 2011b). Chemical analyses indicate a remarkable overlap in the composition of all ignimbrites with 69–71% SiO_2, 3.5–6% K_2O, and 1–1.5% MgO (Folkes et al. 2011b). Both geothermometry and geo-barometry indicate that magma had pre-eruptive temperatures between 780°C and 820°C (Folkes et al. 2011b) at pressures of 1.4–2.7 kbar (i.e., max 10 km depth). Evaluation of the viscosity of melt (crystal free) at conditions reasonable for the CGI (density of rhyodacitic magma at 2.45 g/cm^3; 3–4% H_2O; 3 kb) gives values of $10^{5.9}$–$10^{7.2}$ Pa s (Folkes et al. 2011b). The CGI eruptive temperatures are estimated at maximum of 790°C by the compositions of co-existing Fe–Ti oxides in white pumice (Folkes et al. 2011b).

Fig. 2 **a** Toconquis Group and Cerro Galán ignimbrite at the Rio Las Pitas locality, Vega Real Grande section (*red star* in Fig. 1); **b** valley pond facies of CGI. Note the flat-topped surface (Curuto locality, 27 km west of the caldera); **c** columnar jointing at Curuto; **d**, **e** typical facies of CGI from the base **d** to the top **e** characterized by low pumice (<10%) and lithic (<5%) content (Aguas Calientes locality, sites CG0031 and CG0035; cf. Table 3); **f** CGI basal contact with the underlying Ordovician metasediments (Curuto locality). Note the relevant presence of rip-up clasts; **g** enlargement of previous picture showing imbricated rip-up clasts. Cited localities are in Fig. 1b
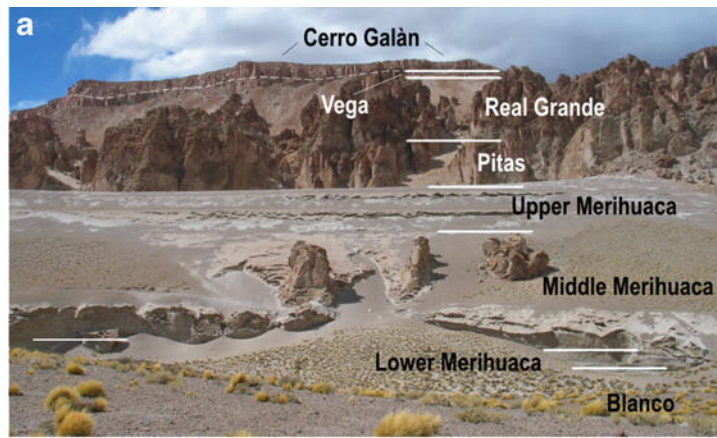
Temperature estimation by paleomagnetic method

The emplacement temperature of pyroclastic flows can be estimated with paleomagnetic methodologies performed on lithic clasts embedded within pyroclastic deposits (McClelland and Druitt 1989). Lithic fragments can be present in various amounts in pyroclastic density currents, either picked up from the magma chamber or conduit walls (accessory lithics), or ripped up along the flow path (accidental lithics). If clasts contain magnetic minerals and are heated up, then they can acquire a new magnetization, as a function of the heating temperature.

When lithic clasts are incorporated into high temperature pyroclastic flows, i.e., higher than the Curie temperature of the magnetic minerals present in the lithic clasts (e.g., 580°C for magnetite), the original magnetization will be completely removed. A new magnetization, oriented parallel to the Earth's magnetic field at the time of emplacement, will be acquired by the clast when its temperature decreases below the blocking temperature (T_b). The T_b is the temperature below which the relaxation of the magnetization becomes slow compared to the investigated time scale, i.e., the TRM is frozen at T_b during cooling in presence of a magnetic field (e.g., Dunlop and Özdemir 1997). Therefore, in clasts embedded in a high-temperature pyroclastic density current, a single magnetic component will be detected, which is parallel in all clasts (Fig. 3a).

When lithic clasts are incorporated into a pyroclastic flow at an intermediate temperature, between the ambient and Curie temperature of the magnetic minerals present in the clasts, they will lose a portion of their original magnetization. This occurs at the unblocking temperature

of the magnetic minerals present in the clast, which, for rapidly cooled flows, is the temperature at which the TRM is lost during laboratory heating. This unblocking temperature is equal to or lower than the maximum temperature of the deposit. During the cooling of the deposit, the clast will acquire a new partial thermoremanence (pTRM), which will partially overprint the original magnetization. In this case, the clast will be characterized by the presence of two components of magnetization: an original, randomly oriented high-temperature component and a new low-temperature component homogeneously oriented parallel to the Earth's magnetic field at the time of the deposit emplacement (Fig. 3b).

The progressive demagnetization technique emulates the natural processes in the opposite direction, heating the samples from ambient to the Curie temperature (T_c) and measuring the magnetic remanence at each thermal step. The demagnetized clasts can show one or two components of magnetization. In the case of two components of magnetization, the intersection temperature of the two components is an estimate of the emplacement temperature, whereas in the case of single component-oriented parallel to the expected magnetic field, the emplacement temperature will be higher than the unblocking temperature (T_{ub}) for each clast.

To validate the use of paleomagnetic techniques for determination of ignimbrite emplacement temperatures, a statistical analysis of magnetization components and their orientations must be completed. At the same time, the potential presence of an overprinting magnetic signature must be evaluated. The process of blocking and unblocking of the magnetization of a lithic clast is a probabilistic process. Grains that are unblocked during the natural heating process may not be similarly unblocked during
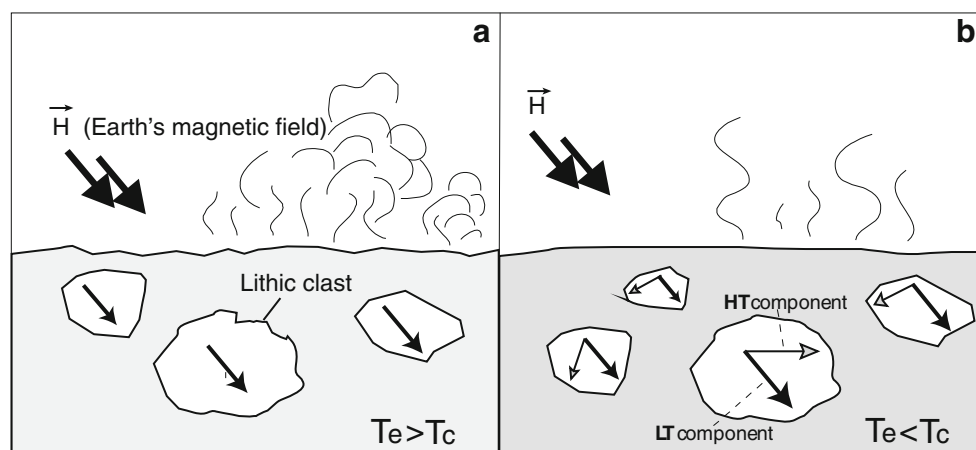
Fig. 3 Schematic representation of remagnetization processes in lithic clasts. a The ignimbrite emplacement temperature T_e is higher than the Curie temperature ($T_e > T_c$) of the magnetic minerals of the lithic clast. The clast will carry a single component magnetization vector oriented along the Earth magnetic field present during cooling; b the

emplacement temperature is lower than the Curie temperature ($T_e < T_c$). The clast will carry two components: a randomly oriented high-temperature (HT) component and a low-temperature (LT) component oriented along the Earth magnetic field (modified after Porreca et al. 2008)

laboratory heating due the difference in time scale between the natural and laboratory processes. In this case, it is important to demagnetize a large number of clasts to produce reliable, significant statistics.

Furthermore, the paleomagnetic signature can be altered by the effects of chemical overprinting (chemical remanent magnetization, CRM) due to field or laboratory alteration (McClelland-Brown 1982; McClelland and Druitt 1989) and by the exposure to the Earth's magnetic field at ambient temperature for a long time (viscous remanent magnetization, VRM). Either or both processes can take place in some clasts, producing new magnetic components that may be erroneously interpreted as pTRM and could lead to false temperature estimations. Moreover, both the CRM and the VRM magnetizations vary strongly as a function of various parameters, such as magnetic mineralogy and grain size. Lithic clasts in the Cerro Galán ignimbrite are very heterogeneous in lithology, and the origin of low-T components could vary for each case. In order to identify the main magnetic carriers and recognize possible chemical magnetic overprint, we have performed a series of rock magnetic measurements on selected samples, which will be described in the next sections.

Finally, in order to distinguish between VRM and pTRM, we follow the approach of Bardot and McClelland (2000) in using the magnetite nomograph by Pullaiah et al. (1975) to determine the relationship between the unblocking temperature (T_{ub}) of a VRM as a function of time. The Pullaiah nomograms refer to single domain magnetite, and in the presence of multi-domain magnetite, the T_{ub} is underestimated. For this reason, they are assumed to provide a minimum value for the emplacement temperature. The relationship is expressed as:

$$T_{ub} = 75 + 15 \log(\text{acquisition time in years}) \tag{1}$$

and is valid for magnetite-bearing components with acquisition times between 10^2 and 10^6 years. As the age of investigated ignimbrites is more than 2 Ma, they have been subjected to a continuous geomagnetic field since 780 ka (i.e., during Brunhes epoch). In this case, the T_{ub} of VRM is limited to this period, and therefore, following the relationship given by Bardot and McClelland (2000), it cannot be higher than 165°C.

Therefore, all the low-temperature components with $T_b <$ 165°C may be potentially due to VRM and are therefore not considered here for temperature estimations. Components with $T_b >$ 165°C are valid for estimation of pTRM.

Sampling and laboratory procedures

The sampling strategy was planned to evaluate changes in flow emplacement temperature with distance from the vent and with stratigraphic height in the flow deposits. We analyzed a total of 301 oriented clasts from 18 localities (Tables 2 and 3); 125 samples were from the Toconquis Group and 176 samples from the Cerro Galán ignimbrite. The samples were collected from proximal to distal localities (52 km) and, in the case of the CGI, at variable azimuth from the vent (Fig. 4a). The Toconquis Group ignimbrites were largely sampled at Rio de las Pitas, Vega Real Grande (star in Fig. 4a), located 12 km west of the caldera in a >250-m-thick section of ignimbrites (Fig. 4b). In particular, the Real Grande ignimbrite was sampled at along Rio de las Pitas locality and in other three additional localities, i.e., about 500 m NW and SE Vega Real Grande and on the eastern slopes of Cerro Ratones, 55 km N of the caldera (Fig. 4a). For clarification, we use the word *locality* to identify a single point on a 1:25,000 map while a *site* is an outcrop of about 1 m^2, where lithic clasts were sampled.

Samples were collected at different stratigraphic heights in the CGI in order to eventually identify temperature stratifications. At Aguas Calientes, five sites (CG0031–CG0035) were sampled; in Antofagasta, four sites were sampled (CG0371–CG0374, Table 3); and at Los Nacimientos and at Puntas Gordas, three sites were sampled (CG0342–CG0344 and CG0351–CG0353, respectively). Site locations are in Fig. 4a, and sections height and distances from caldera rim are reported in Table 3, for each site. At Paycuqui, five sites were sampled at each of two sections (CG0201–CG0205 and CG0281–CG0285; see also Wright et al. 2011a). Finally, three sites were sampled in the CGI subunits at the distal locality of Tacuil (sites CG0420, CG0430, and CG0440).

The clast population is variable in lithology, including dominant plagioclase-phyric dacite (ppd) clasts, found in almost all outcrops, and subordinate metavolcanics, metasediments, quartzites, and amphibolites. In most cases, the lithic clast lithologies reflect the lithologies of the substrate upon which the ignimbrite was emplaced. The substrate is dominated by slightly deformed Ordovician rocks (metavolcanics, mica-schists, and low-grade metasediments) in the western sector and by lower Paleozoic crystalline units in the eastern sector (granitoids and orthogneisses; Kay et al. 2008). ppd are not encountered in outcrop outside the caldera, and its ubiquitous presence can be related to a proximal emplacement of dacitic lavas around the caldera or to an intracaldera dome.

We therefore conclude that, excluding ppd clasts, lithic clasts are mostly accidental, ripped up from the ground surface during transport of the flow, and the proportion of clasts that are inferred to originate from the chamber walls or the conduit margins is small. This association is particularly useful for TRM studies of the emplacement temperatures of ignimbrites because the

Table 2 Toconquis Group site TRM results

Unit	Site (ID)	Latitude	Longitude	Locality	Facies	h asl (m)	Distance (km)	N	Nr	Class A	Class B	T_{ub} (°C)	T_e
Vega	TC0264	679052	7125434	Vega Real Grande	Proximal	4,470	12	5	5	5		>580	
Real Grande	TC0192	682369	7122876	SE Rio las Pitas	Proximal	4,710	9	2	2	2		>580	
	TC0263	679052	7125434	Vega Real Grande	Proximal	4,423	9	3	3	3		>600	
	TC0262	679052	7125434	Vega Real Grande	Proximal	4,383	9	6	6	6		>600	
	TC0261	679052	7125434	Vega Real Grande	Proximal	4,363	12	3	3	3		>580	
	TC0305	676765	7126380	NW Rio las Pitas	Proximal	4,323	15	1	1	1		>580	
	TC0303	676765	7126380	NW Rio las Pitas	Proximal	4,341	15	1	1	1		>580	
	TC0302	676765	7126380	NW Rio las Pitas	Proximal	4,357	15	2	2	2		>580	
	TC0171	676290	7125803	NW Rio las Pitas	Proximal	4,229	15	2	2	2		>580	
	TC0620	717467	7201067	The Ratone's Saddle	Distal	4,050	55	6	6	6		>600	
Pitas	TC0251	679052	7125434	Vega Real Grande	Proximal	4,343	12	4	4	4		>620	
	TC0215	678932	7124869	Vega Real Grande	Proximal	4,333	12	6	6	6		>600	
	TC0770	679034	7124976	Vega Real Grande	Proximal	4,320	12	8	8	8		>610	
	TC0241	678842	7125054	Vega Real Grande	Proximal	4,284	12	6	6	6		>620	
	TC0780	678842	7125054	Vega Real Grande	Proximal	4,280	12	1	1		1		610–630
Upper Merihuaca	TC0750	679034	7124976	Vega Real Grande	Proximal	4,305	12	8	7	6	1	>610	530–560
	TC0231	678842	7125054	Vega Real Grande	Proximal	4,303	12	4	3	3		>620	
	TC0214	678932	7124869	Vega Real Grande	Proximal	4,295	12	4	3	3		>580	
	TC0222	678661	7125002	Vega Real Grande	Proximal	4,290	12	4	3	3		>640	
Middle Merihuaca	TC0221	678661	7125002	Vega Real Grande	Proximal	4,286	12	3	3	3		>600	
	TC0740	679034	7124976	Vega Real Grande	Proximal	4,275	12	10	10	10		>610	
	TC0161	678822	7124946	Vega Real Grande	Proximal	4,260	12	5	5	5		>580	
	TC0162	678822	7124946	Vega Real Grande	Proximal	4,255	12	2	2	2		>580	
	TC0213	678932	7124869	Vega Real Grande	Proximal	4,245	12	6	5	4	1	>600	360–480
Lower Merihuaca	TC0212	678932	7124869	Vega Real Grande	Proximal	4,230	12	6	6	4	2	>630	580–600
	TC0730	678932	7124869	Vega Real Grande	Proximal	4,230	12	10	10	4	6	>610	590–610
Blanco	TC0211	678932	7124869	Vega Real Grande	Proximal	4,226	12	7	7	7		>580	

acquired TRM of accidental clasts is related to the pyroclastic flow temperature and not to lengthy pre-heating in the conduit. Lava clasts and metavolcanics were preferentially sampled over other lithic types because they are more common and provide more reliable paleomagnetic results than other lithologies; they represent 60% and 20% of the total sampled lithologies, respectively. Average clast sizes in the deposit range from 0.5 to 10–15 cm.

At each site, we sampled from three to ten clasts (Tables 2 and 3), except in case of very low lithic percentages (<1% of deposit) where less than three clasts were sampled. The strike and dip of each clast were measured in the field with a magnetic compass. The magnetic deviation induced by the deposit on the compass was tested and was determined not to influence the paleomagnetic study, i.e., the identification of the number of components of magnetization and their orientations with respect to the geocentric axial dipole (GAD) geomagnetic

field. Most of the clasts were not larger than 4 cm, with an average diameter of ~1.5 cm. For some larger clasts (5–20 cm in diameter), subsamples were cut from the core and rim to evaluate the presence of a temperature gradient within biggest clasts.

The oriented clasts (or subsamples of clasts) were embedded in white non-magnetic plasticine, which was placed into a rigid plastic cylinder with standard dimensions (diameter $\varphi=25$ mm, height $h=22.5$ mm) in the laboratory, following the procedure adopted by Cioni et al. (2004). Paleomagnetic analyses and rock magnetic analyses were performed at the Paleomagnetic Laboratory of University of Roma Tre; rock magnetic analyses of some representative samples were also carried at the Paleomagnetic Laboratory of ETH-Zurich.

In order to identify the mineralogy of the main magnetic carriers and to assess whether any mineralogical alteration has affected our temperature estimates, we have performed

Table 3 Cerro Galán site TRM results

Site (ID)	Latitude	Longitude	Locality	Facies	h asl (m)	Distance (km)	N	N_r	Class		T_{ub} (°C)
									A	B	
CG0012	715162	7198326	Hombre Muerto	Distal	4,025	52	2	2	2	/	>610
CG0013	715162	7198326	Hombre Muerto	Distal	4,043	52	3	3	3	/	>580
CG0021	714430	7159589	Rio de los Patos	Proximal	4,250	14	1	1	1	/	>520
CG0031	713403	7160446	Aguas Calientes	Proximal	4,112	10	5	5	5	/	>520
CG0032	713403	7160446	Aguas Calientes	Proximal	4,135	10	4	4	4	/	>580
CG0033	713403	7160446	Aguas Calientes	Proximal	4,151	10	6	6	6	/	>600
CG0034	713403	7160446	Aguas Calientes	Proximal	4,172	10	3	3	3	/	>520
CG0035	713403	7160446	Aguas Calientes	Proximal	4,190	10	3	2	2	/	>580
CG0041	691417	7172849	Dique Trapiche	Medial	4,122	28	1	1	1	/	>580
CG0042	691417	7172849	Dique Trapiche	Medial	4,141	28	1	1	1	/	>520
CG0051	692242	7167984	Stonhenge	Medial	4,434	24	3	3	3	/	>580
CG0201	663963	7132027	Paicuqui	Medial	3,619	27	9	5	5	/	>600
CG0202	663963	7132027	Paicuqui	Medial	3,629	27	5	5	5	/	>580
CG0203	663963	7132027	Paicuqui	Medial	3,632	27	8	8	8	/	>580
CG0204	663963	7132027	Paicuqui	Medial	3,640	27	3	3	3	/	>580
CG0205	663963	7132027	Paicuqui	Medial	3,619	27	3	2	2	/	>580
CG0271	657459	7118286	NW Antofagasta	Distal	3,463	34	4	4	4	/	>580
CG0272	657459	7118286	NW Antofagasta	Distal	3,400	34	4	4	4	/	>600
CG0281	664646	7132471	Paicuqui	Medial	3,650	27	7	7	7	/	>620
CG0282	664646	7132471	Paicuqui	Medial	3,606	27	6	5	5	/	>580
CG0283	664646	7132471	Paicuqui	Medial	3,645	27	6	1	1	/	>580
CG0284	664646	7132471	Paicuqui	Medial	3,630	27	3	3	3	/	>580
CG0285	664646	7132471	Paicuqui	Medial	3,645	27	5	3	3	/	>600
CG0342	663447	7143733	Los Nacimientos	Distal	3,879	30	6	2	2	/	>600
CG0343	663447	7143733	Los Nacimientos	Distal	3,879	30	5	4	4	/	>580
CG0344	663447	7143733	Los Nacimientos	Distal	3,879	30	4	4	4	/	>580
CG0351	675484	7150230	Puntas Gordas	Distal	4,295	22	5	5	5	/	>610
CG0352	675484	7150230	Puntas Gordas	Distal	4,295	22	6	6	6	/	>610
CG0353	675484	7150230	Puntas Gordas	Distal	4,300	22	3	3	3	/	>610
CG0371	659131	7116841	Antofagasta	Distal	3,445	33	4	4	4	/	>580
CG0372	659132	7116842	Antofagasta	Distal	3,450	33	2	2	2	/	>610
CG0373	659133	7116843	Antofagasta	Distal	3,458	33	5	4	4	/	>580
CG0374	659134	7116844	Antofagasta	Distal	3,465	33	5	2	2	/	>630
CG0381	674833	7091114	Rio el Jote	Distal	3,504	31	4	4	4	/	>600
CG0382	674833	7091114	Rio el Jote	Distal	3,520	31	4	3	3	/	>550
CG0420	753733	7169457	Tacuil	Distal	2,718	44	4	3	3	/	>630
CG0430	753733	7169457	Tacuil	Distal	2,718	44	6	5	5	/	>600
CG0440	753733	7169457	Tacuil	Distal	2,718	44	8	8	8	/	>600
CG0460	757643	7155690	Hualfin	Distal	2,930	43	3	3	3	/	>630
CG0660	676278	7158826	Beltran Runup	Distal	4,410	27	7	7	7	/	>600

Sampled sites are ordered from the lowest to the highest in the stratigraphic section, for each Toconquis unit. We include site (ID), coordinates, locality name, distal/proximal facies, height a.s.l., distance from the present caldera margins (measured at the intersection with the site-caldera centre connecting line), number of analyzed samples, number of reliable samples, number of samples classified as class A or class B, unblocking temperatures, and temperature interval between LT component and HT component in class B samples. In the case of more than one B sample at the same site, the reported values are the lowest and highest measured temperatures
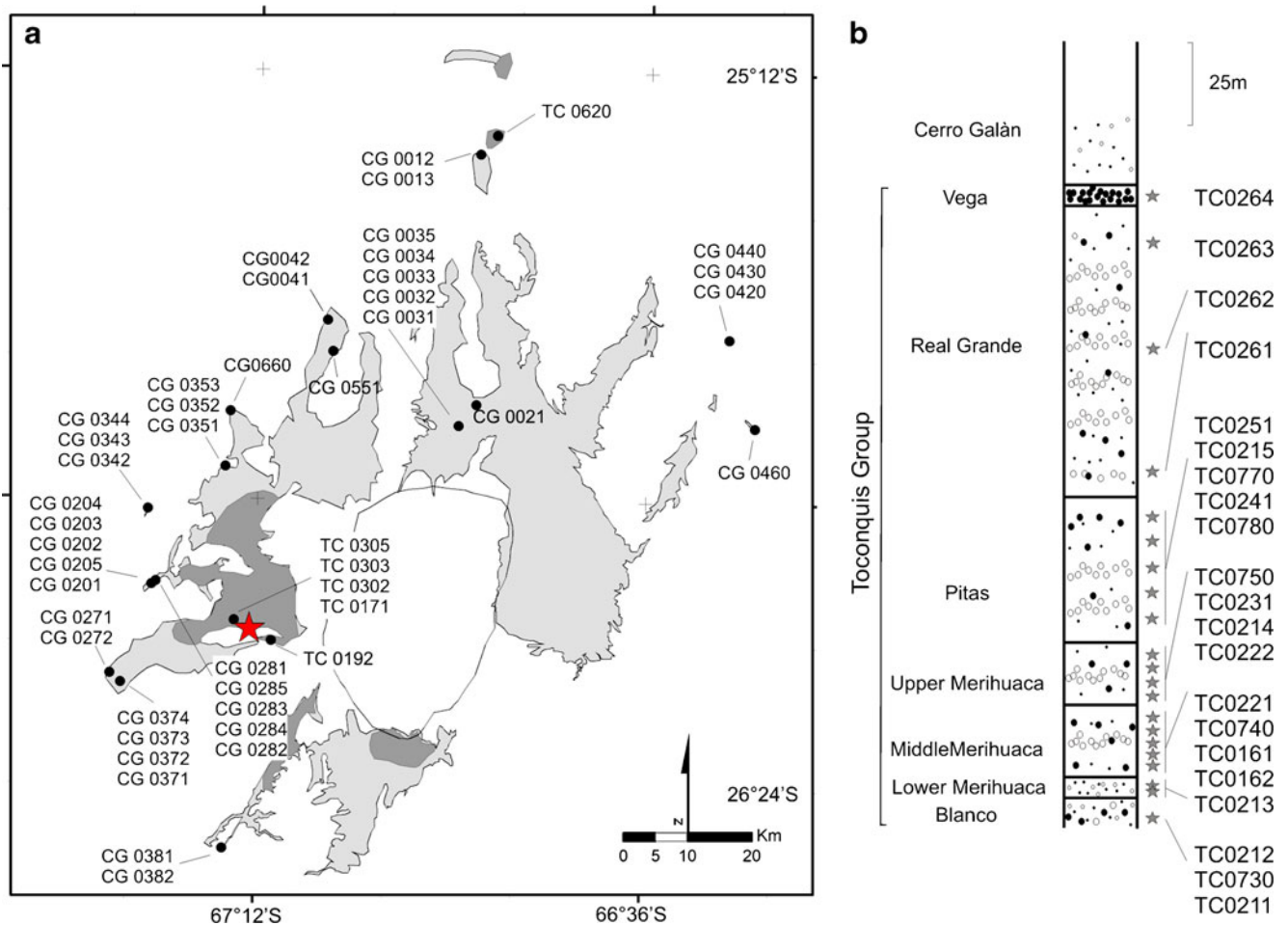
Fig. 4 Sampling site locations. **a** The areal extent of the Cerro Galán ignimbrite is shown in *light gray*; in *dark gray* is the areal extent of the underlying Real Grande ignimbrite. *CG* Cerro Galán ignimbrite, *TC* Toconquis Group ignimbrites. **b** Stratigraphic log of the >250-m section at Rio Las Pitas, Vega Real Grande section (*red star symbol*); sampling sites along the log are represented by *gray stars*. Note that TC sampling sites outside Rio Las Pitas section are Real Grande ignimbrite sampling sites

rock magnetic analyses on 15 representative samples (except thermomagnetic analyses, which were performed on 14 samples). The analyzed samples were obtained by eight dacites, four metavolcanics, two metasediments, and a quartzite clast. Rock magnetic measurements include (a) determination of isothermal remanent magnetization (IRM) that allows the definition of the saturation field and the coercivity of remanence (H_{cr}); (b) thermal unblocking of a composite three-component isothermal remanent magnetization (composite IRM) that allows to identify the contribution of the soft, medium, and hard coercivity mineral fractions and the relative mineralogical phases; and (c) thermomagnetic analysis of high-temperature magnetic susceptibility measured in air, in order to identify the Curie temperature of the main magnetic carriers and to detect any mineralogical alteration during heating. The rock analyses are performed on powdered samples, and only six out of 15 lithic clasts were large

enough to allow the cutting of samples both for rock analysis and TRM analysis.

The conditions for determination of IRM include a progressive increase in the imposed magnetizing field, using an ASC impulse magnetizer, and the measurements of the remanent magnetization at each incremental step by a JR-6A spinner magnetometer. Samples were firstly saturated in a 2,000-mT magnetic field along the $-z$ sample direction, and then an IRM was acquired stepwise in nine steps from 50 to 2,000 mT in an antipodal field ($+z$). This procedure provides information on the field needed to saturate the magnetization as well as the coercivity of remanence ($H_{cr'}$). The three-component IRM was then thermally demagnetized in 13 steps on the same samples, according to the procedure reported by Lowrie (1990). Minimum, intermediate, and maximum magnetic fields of 120, 600, and, 1,700 mT respectively, were applied to the *x*-, *y*-, and *z*-axes of the samples.

In order to define the Curie temperature of the magnetic minerals and to exclude the presence of thermal mineralogical alteration, magnetic susceptibility was measured as a function of temperature in air, from room temperature to 700°C, in a heating–cooling cycle on ~2 cm^3 of powdered sample. This kind of measurement was made using AGICO CS-2 furnace apparatus. Finally, the textural relationships between magnetic and non-magnetic mineral phases were determined using thin sections of eight representative lithic samples, selecting the most common lithologies (dacite, metavolcanics, metasediments, and quartzites).

The natural remanent magnetization (NRM) was measured using a JR-6A spinner magnetometer on 301 specimens. Six of these specimens were also analyzed for magnetic rock determination, and in other five clasts, two specimens were obtained from each one, at the rim and core of the clast. Thermal demagnetization was carried out using an external field shielded furnace with residual fields <10 nT in 13–17 thermal steps, reducing the temperature steps from 50°C to 20°C at higher temperature. Magnetic susceptibility was also measured at each thermal step by the KLY-3 Kappabridge instrument to detect any possible mineralogical changes during the heating process.

Magnetic remanence data were plotted on a Zijderveld orthogonal demagnetization diagram (Zijderveld 1967) and the Remasoft 3.0 software was used to identify the principal magnetic components (Chadima and Hrouda 2006). The number of remanence components was defined by evaluating maximum angular deviation (MAD) values of the each single vector. A maximum of 10° was accepted as a limit of reproducible result for a single component. Paleomagnetic mean directions for each site and ignimbrite unit are made applying Fisher statistics (Fisher 1953). The best estimates of the dispersion, k, and the direction reliability evaluated at the 95% confidence level, α_{95}, have been also calculated for each ignimbrite unit.

Results

Rock magnetic data

The acquired IRM curves for our samples show a rapid increase in IRM over the low magnetic field range (Fig. 5). Furthermore, 95% saturation is reached at 350–400 mT in most of the analyzed samples (Fig. 5). This behavior is characteristic of low-coercivity magnetic grains, such as titanomagnetite and/or magnetite (e.g., Dunlop and Özdemir 1997). In addition, the remanent coercivity ($H_{cr'}$) values of these samples ranges from 35 to 75 mT (Fig. 5), which typically represent values of low-coercivity minerals (e.g., Dunlop and Özdemir 1997). In contrast, four samples do not reach magnetic saturation at the maximum applied field (2,000 mT), suggesting that these samples contain high-coercivity minerals, such as hematite.

Using composite (three components) IRM and thermal demagnetization, we confirm the predominance of low-coercivity minerals. The IRM values of the x, y, and z components (soft, medium, and hard fractions) indicate the relative proportion of each component. Figure 6 shows that the soft fraction (coercivity <0.2 T) predominates in all samples. Using thermal demagnetization, we find that this low-coercivity component is stable up to 580°C, indicating that magnetite is the main magnetic carrier (e.g., Dunlop and Özdemir 1997; Fig. 6a). Some samples are characterized by IRM drops at 580°C and between 350°C and 400°C (Fig. 6b), suggesting the presence of magnetite/Ti-poor titanomagnetite and probably maghemite, respectively. The proportionally minor, medium, and hard fractions (up to 20% of soft fraction) generally remain

Fig. 5 Isothermal remanent magnetization (*IRM*) analyzed in 15 representative samples. Ninety-five percent saturation is reached at 350–400 mT in most of the analyzed samples except in four samples that do not reach saturation at the maximum applied field (2 T). The overall remanent coercivity $H_{cr'}$ is between 35 and 75 mT
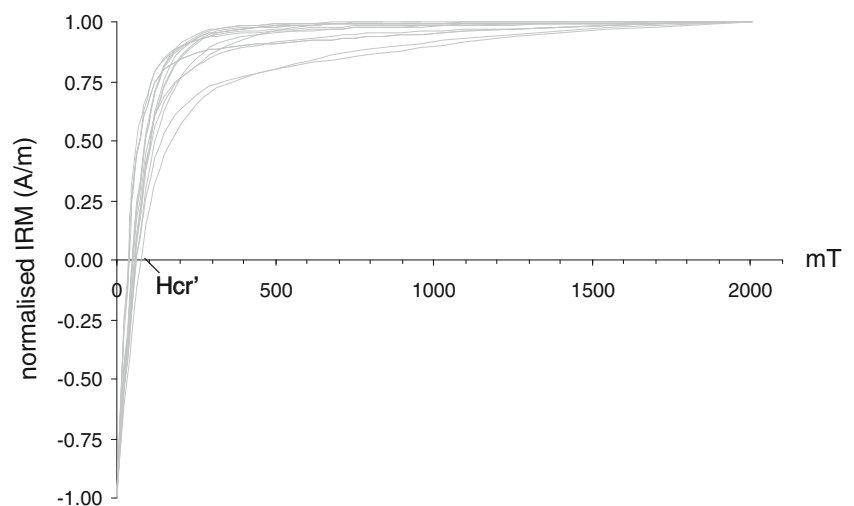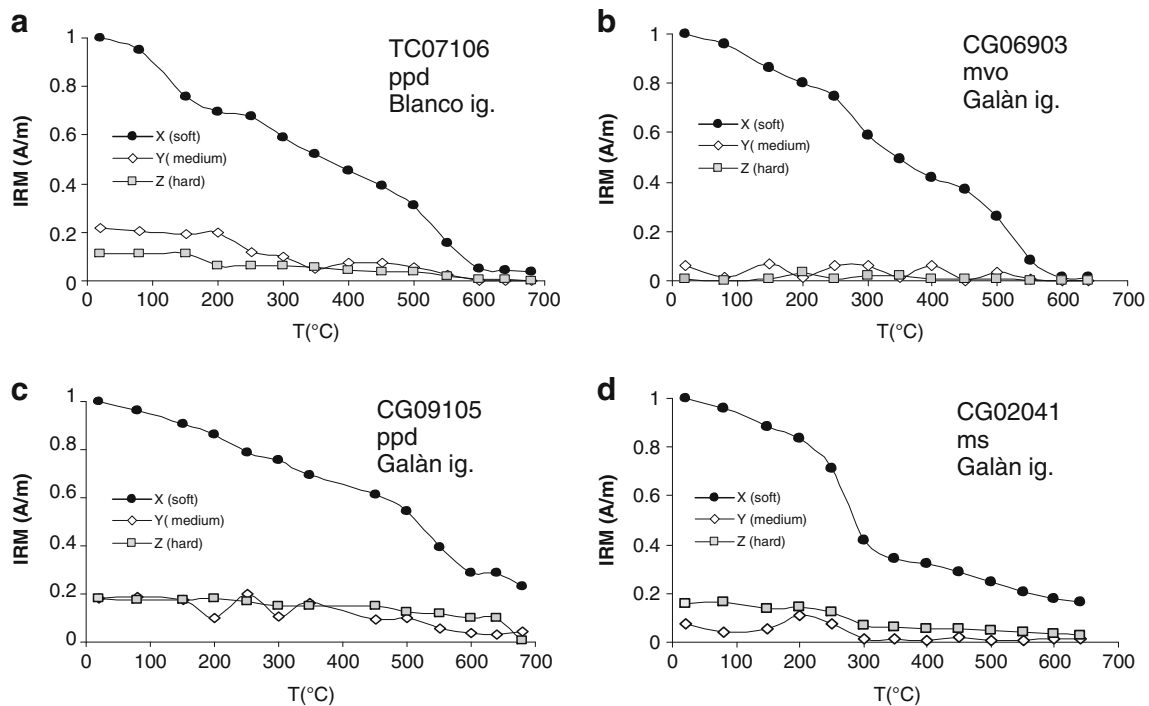
Fig. 6 Representative composite IRM decay for four samples. The soft fraction prevails in all the 15 analyzed samples. **a** Soft fraction decay at 580°C is indicative of the presence of magnetite; **b** smooth step at 300–400°C in the soft fraction can be indicative of maghemite and titanomagnetite; **c** the hard fraction is at about 20% of the soft fraction and decays at about 680°C revealing low content of hematite; **d** the soft fraction decay by 40% at about 300°C can reveal the presence of iron sulfides as secondary magnetic mineral in metasediments. *ppd* plagioclase phyric dacite, *mvo* metavolcanic Ordovician, *ms* mica-schist

stable up to 680°C (Fig. 6c), suggesting the presence of hematite in some samples. Metasediment samples are characterized by a soft fraction decay at ~300°C, which could be related to the presence of iron sulfides (e.g., Weaver et al. 2002; Fig. 6d and the relative thermomagnetic curve in Fig. 7f). Iron sulfides can be present as secondary minerals in metasediments as for the shown sample.

The thermomagnetic curves made on 14 clasts confirm the presence of different minerals as a function of clast lithology (Fig. 7). One sample did not give reliable results. In the rest of the analyzed samples, the heating and the cooling curves are reversible, except for three samples. In these three samples, from different lithologies, the susceptibility of the cooling curve is remarkably higher than the heating curve, indicating that some oxidation has occurred during the heating process (e.g., Fig. 7f). In 12 samples, the susceptibility drops to zero between 580°C and 600°C, which is the Curie temperature of magnetite (Fig. 7a–c). Five samples also show a susceptibility deflection at 300–400°C, indicating the presence of another low T_b magnetic carrier, likely maghemite (Fig. 7d). In two dacite samples, the susceptibility drop occurs between 600°C and 620°C, confirming the presence of hematite as a magnetic carrier (Fig. 7e). In Fig. 7f, the scale vertical enlargement

highlights a drop in the 300–400°C interval in the susceptibility heating curve that can be ascribed to the presence of iron sulfides.

The presence of hematite can be related to oxidation processes in lithic clasts before or after emplacement of the ignimbrite. If the oxidation is related to the pre-emplacement history of the clasts, then temperature estimations are valid. In contrast, if the oxidation occurred after emplacement, then a chemical remanent magnetization could totally overprint the original magnetization acquired during emplacement of the ignimbrite.

In order to verify this possibility, we examined thin sections of representative hematite-bearing red colored and black non-oxidized plagioclase-phyric dacite clasts. The presence of iron–titanium oxide alteration was also highlighted by Francis et al. (1983), who found that some of the investigated Fe–Ti oxides were altered or exsolved in the matrix. We find that oxidation has involved relict grains of biotite and other iron-bearing minerals, which appear weakly folded. The oxidation event is therefore interpreted to have occurred during deformation of the clast, before it was involved in the eruption. Moreover, it is important to note that both oxidized and non-oxidized clasts are present at the same sites (e.g., site CG0342 in "Appendix 2") and both clast

Fig. 7 Representative thermo-magnetic curves. Most of the 14 analyzed samples show good correlation between heating and cooling curves, indicating that there is no mineral formation during the heating process; steep decays represent Curie temperatures of magnetic minerals; **a**, **b** Curie temperatures at 580°C indicate the presence of magnetite; **c**, **d** deflection at 300–400°C can indicate the presence of maghemite; this behavior occurred in three dacites and two metavolcanics; **e** Curie temperature at 620°C indicates the presence of hematite; **f** peak at 580°C in the heating curve and abrupt increase in the cooling curve suggest new mineralogical phase growing during heating; this behavior is shown by two samples. *ppd* plagioclase-phyric dacite, *bppd* black plagioclase-phyric dacite, *mvo* metavolcanic Ordovician, *ms* mica-schist
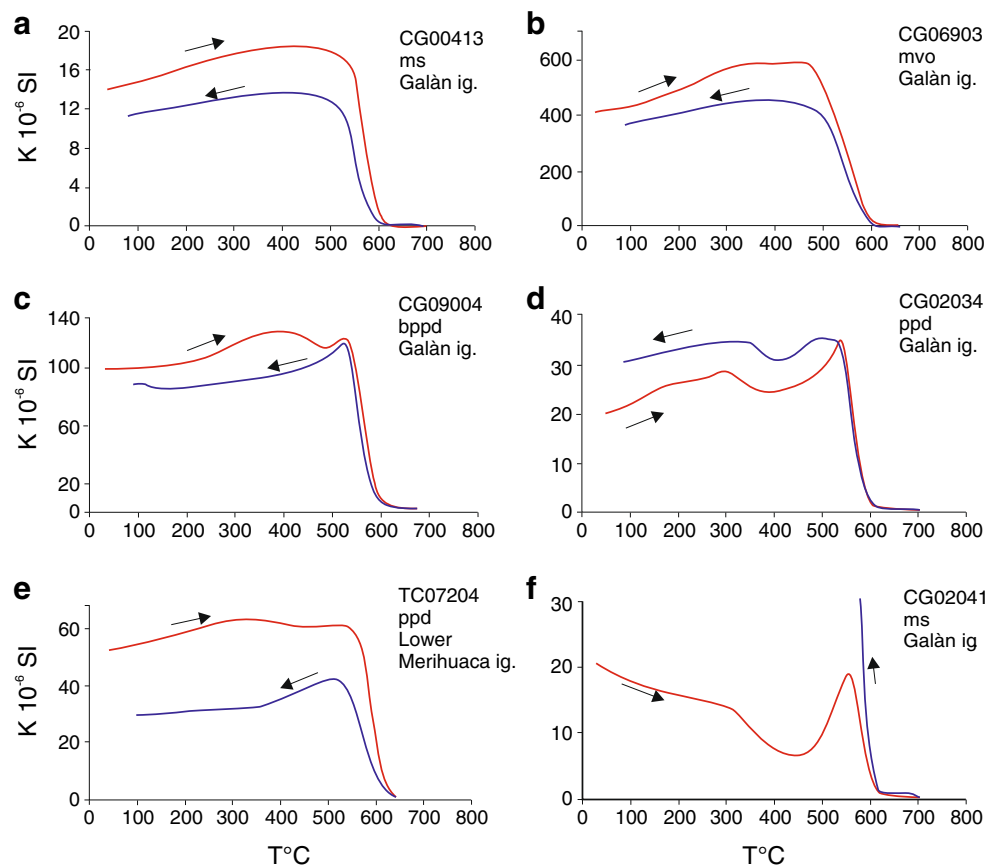
types are characterized by a single component oriented close to the GAD magnetic field. This confirms that dacite clasts oxidation has occurred before the emplacement of ignimbrite, validating the temperature evaluation. Moreover, the reversibility of the thermomagnetic curve in presence of hematite (cf. Fig. 7e) excludes the possibility that hematite formation is induced by thermal alteration of the lithic magnetic mineralogy during laboratory thermal demagnetization.

Thermal remanent magnetization results

The NRM of all the analyzed samples, normalized to the standard 10-cm^3 volume specimen, is highly variable, ranging from 2.4×10^{-3} to 79 A/m, where dacite samples show slightly higher values than other lithic types. The remanent magnetization is usually removed at temperatures >580°C, and the paleomagnetic behavior is stable in most cases. Four samples from the Toconquis Group and 20 samples from Cerro Galán Ignimbrite ("Appendix 1" and "Appendix 2") show unstable behavior and therefore have not been considered in the statistics.

To discriminate between the magnetic signatures of different clasts, we classified the specimens by the number of magnetic components and their orientation, following the

demagnetization pattern classification reported in McClelland et al. (2004) but using different class names (Tables 2, 3, and 4). Class A specimens (e.g., Fig. 8a) show a single magnetization component vector. Class B specimens show two components, one stable at high temperatures (HT component) and one at low temperatures (LT component). The LT component is consistent with the GAD geomagnetic field, whereas the HT component is randomly oriented. The GAD at Cerro Galán today has an inclination of −22°; the 2.08-Ma Cerro Galán Ignimbrite (Kay et al. 2011) is expected to have had a reverse magnetic polarity, producing positive inclination. For the Toconquis Group, the expected magnetic polarity is variable for each unit. According to biotite ^{40}Ar/^{39}Ar ages of Folkes et al. (2011a), Lower, Middle, and Upper Merihuaca ignimbrites should have reverse polarity, whereas the Pitas, Real Grande, and Vega ignimbrites should have normal polarity (based on polarity subchrons of Gradstein et al. 2004).

Results for the Toconquis Group ignimbrites

The Toconquis Group includes seven ignimbrite units; each of them was analyzed by thermal demagnetization of lithic clasts. The NRM intensity varies from 2.4×10^{-3} to 0.2 A/m, with very few samples showing values up to 3 A/m.

Individual sample results are shown in "Appendix 1," while composite results for each Toconquis unit are described below (Fig. 8; Table 4).

In the Blanco ignimbrite, all seven demagnetized samples show a single magnetic component vector stable up to 580°C (Fig. 8a). Subsamples from the core and rim of a 10-cm clast were also analyzed, and both of the subsamples show a single normally directed component, completely demagnetized (T_{ub}) at 520°C. This component is upward-oriented in all clasts, and its direction is almost close to the present geomagnetic field, thereby all clasts in the Blanco ignimbrite are classified class A. The mean paleomagnetic direction for this unit is $D=26.3°$ and $I=−22°$ (Fig. 9a). The high angle of α_{95} is due to poor number of analyzed clasts.

In the Lower Merihuaca ignimbrite, 16 clasts were demagnetized. Half of these clasts show a single magnetic component, while the other half shows two magnetic components. The single component samples are completely demagnetized at temperatures between 530°C and 630°C, and their direction is close to the actual magnetic field (class A), with normal polarity. The mean paleomagnetic direction is $D=6.3°$ and $I=−45.4°$ (Fig. 9b). In the samples with two components of magnetization (Fig. 8b), the LT component is upward-oriented with $D=8.4°$ and $I=−45.6°$ (Fig. 9c), whereas the HT component is randomly oriented (Fig. 9d). These samples are grouped as class B and the temperatures of separation between LT and HT components vary within a small range from 580°C to 610°C. The emplacement temperature of the Lower Merihuaca unit can therefore be constrained in a range of 30°, while for all the other units, the estimates are for a *minimum* emplacement temperature.

The 26 lithics sampled in the Middle Merihuaca ignimbrite show low NRM, less than 0.1 A/m. One sample did not give reliable results, and therefore, it was not used for statistics. Twenty-five samples show a single component demagnetization vector (class A, Fig. 8c), while one sample shows two

components (class B). Most of class A clasts are completely demagnetized at 580°C, and their mean paleomagnetic direction is $D=8.1°$ and $I=−45.1°$ (Fig. 9e).

In the Upper Merihuaca ignimbrite, 20 samples were thermally demagnetized, with four samples failing to yield stable demagnetization trajectories. Fifteen samples show a single component of magnetization oriented downward (i.e., reverse polarity), except one oriented upward (i.e., normal polarity) and are all demagnetized between 580°C and 620°C. The clasts are therefore classified as class A (Fig. 8d), and the orientation of the mean direction of this component is $D=196.5°$ and $I=48.0°$ (Fig. 9f). One sample shows two component demagnetization vectors. In this sample, the temperature of separation between LT and HT components is in the range of 530–560°C, and it is totally demagnetized at 590°C.

The Pitas ignimbrite was studied by the thermal demagnetization of 25 lithics. Except one sample, all clasts were demagnetized at temperatures between 580°C and 640°C and show a single vector component (class A, Fig. 8e) directed $D=15°$ and $I=−42.2°$ (Fig. 9g). The remaining sample is stable up to 650°C and shows two components of magnetization. The LT component, stable up to 610°C, is directed $D=30°$ and $I=−38°$.

In the Real Grande ignimbrite, 26 samples were demagnetized. All the lithics show a single component demagnetization vector (class A, Fig. 8f), stable between 520°C and 630°C and oriented at $D=9.7°$ and $I=−44.4°$ (Fig. 9h). Finally, the five lithic clasts sampled in the Vega ignimbrite show a single component demagnetization vector (class A, Fig. 8g) directed downward at $D=175.8°$ and $I=48.6°$ (Fig. 9i) and stable up to 560°C.

Results for the Cerro Galán ignimbrite

The NRM of the 176 analyzed lithic clasts from the Cerro Galán Ignimbrite range between 4×10^{-3} and 79 A/m. The principal component analysis applied to the thermal

Table 4 Group statistics for Cerro Galán and Toconquis Group ignimbrites

Fields are the same as in Table 2. *N*, Nr, class, Dec; Inc, α_{95}, *R*, and *k* are reported for each unit. Relative plots in Figs. 9 and 11

N number of samples, *Nr* number of reliable samples, *class* classification, *Dec; Inc* paleomagnetic mean direction, α_{95} semi-angle of 95% confidence, *R* resultant length vector, and *k* dispersion

Unit	N	Nr	Class	Dec.	Inc.	α_{95}	R	k
Cerro Galan	176	150	A	182.9	49.9	5	128	7
Vega	5	5	A	175.8	48.6	31	4	7
Real Grande	26	26	A	9.7	−44.4	15	21	5
Pitas	25	24	A	15.0	−42.2	11	22	8
Upper Merihuaca	20	15	A	196.5	48.0	21	12	4
Middle Merihuaca	26	25	A	8.1	−45.1	10	22	10
Lower Merihuaca	16	8	A	6.3	−45.4	28	7	5
		8	B-Low Tb	8.4	−45.6	12	8	23
			B-High Tb	311.5	−26.1	98	3	1
Blanco	7	7	A	26.3	–22	35	5	4
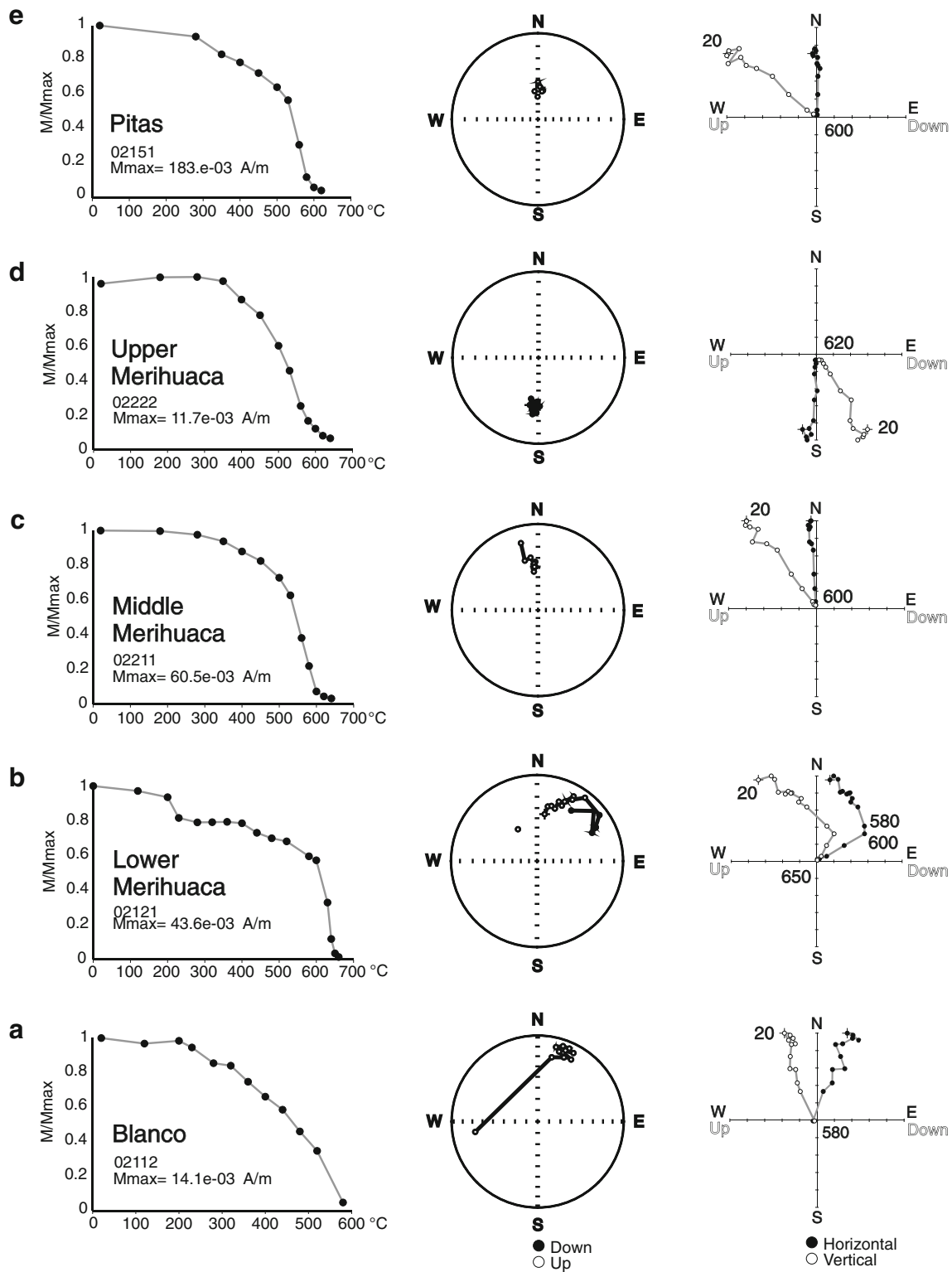
Fig. 8 Thermal demagnetization data for some representative samples of Toconquis Group units (**a**–**g**). For each sample, intensity decay, equal area stereonet, and Zijderveld diagrams are shown. *Left* Normalized intensity decay curve; *middle* equal area projection (*solid dots* lower hemisphere; *open dots* upper hemisphere); *right* orthogonal plots (declination: *black dots on the horizontal plane*; apparent inclination: *white dots on the vertical plane*); numbers are temperature values in degree Celsius. Sample references in "Appendix 1"
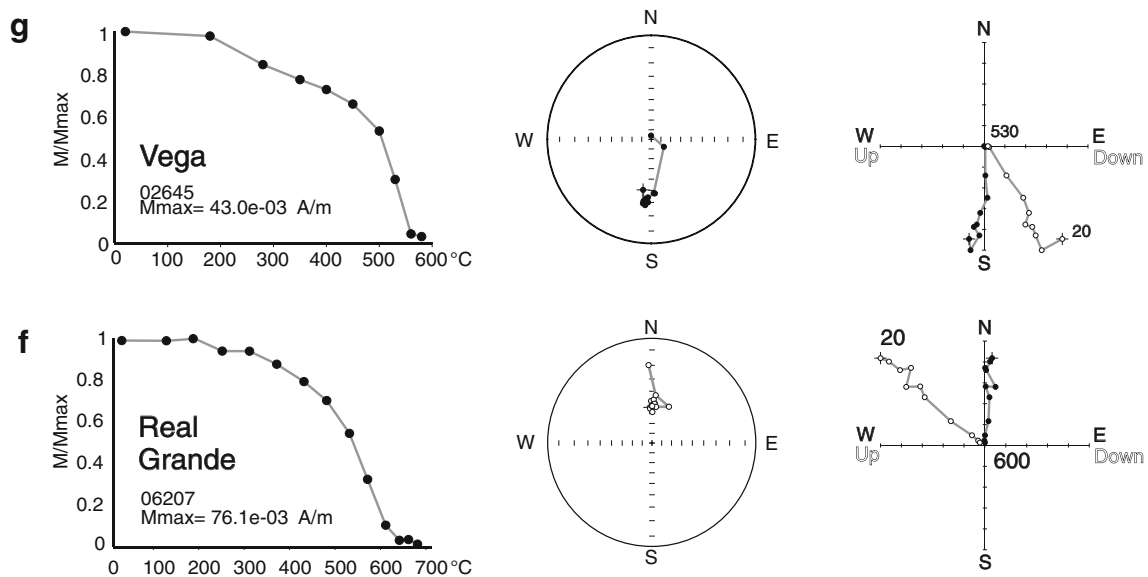
Fig. 8 (continued)

demagnetization results identified magnetization components with MAD usually less than 5°.

Most of the analyzed specimens, 150 out of 176 demagnetized clasts, show a single component demagnetization vector (class A; Fig. 10a–c). The mean direction of this component, shown in Fig. 11, is well-defined and oriented $D=182.9°$ and $I=49.9°$. The minimum and maximum demagnetization temperatures are 440°C and

680°C, respectively, but most of the samples (97%) are completely demagnetized between 520°C and 620°C. Twenty-six specimens were not considered in the mean direction evaluation, as they showed anomalous demagnetization paths or did not demagnetize.

Four lithic clasts from the Cerro Galán ignimbrite were analyzed by TRM analysis at the rim and at the core. In two clasts, the core results are not reliable, while the external
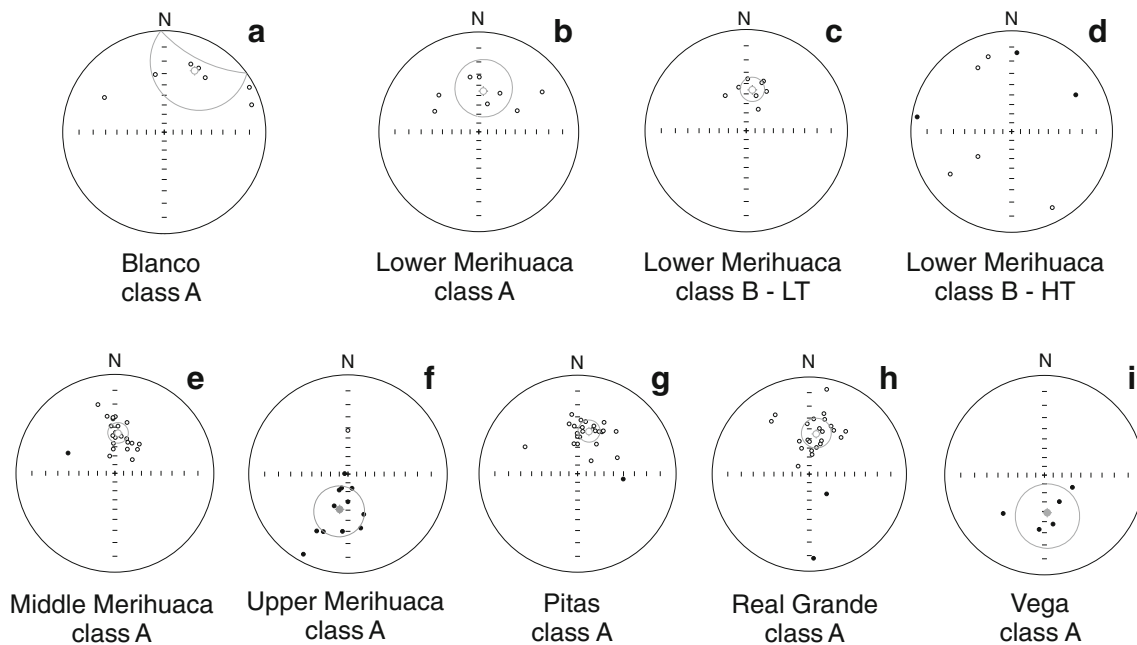
Fig. 9 Equal area stereonets of mean remanence directions of the Toconquis Group units (a–i). *Open symbols* are vectors projected into the upper hemisphere; *filled symbols* represent vectors projected onto the lower hemisphere. *Small and large gray circles* are mean paleomagnetic directions and α_{95} ellipses, respectively
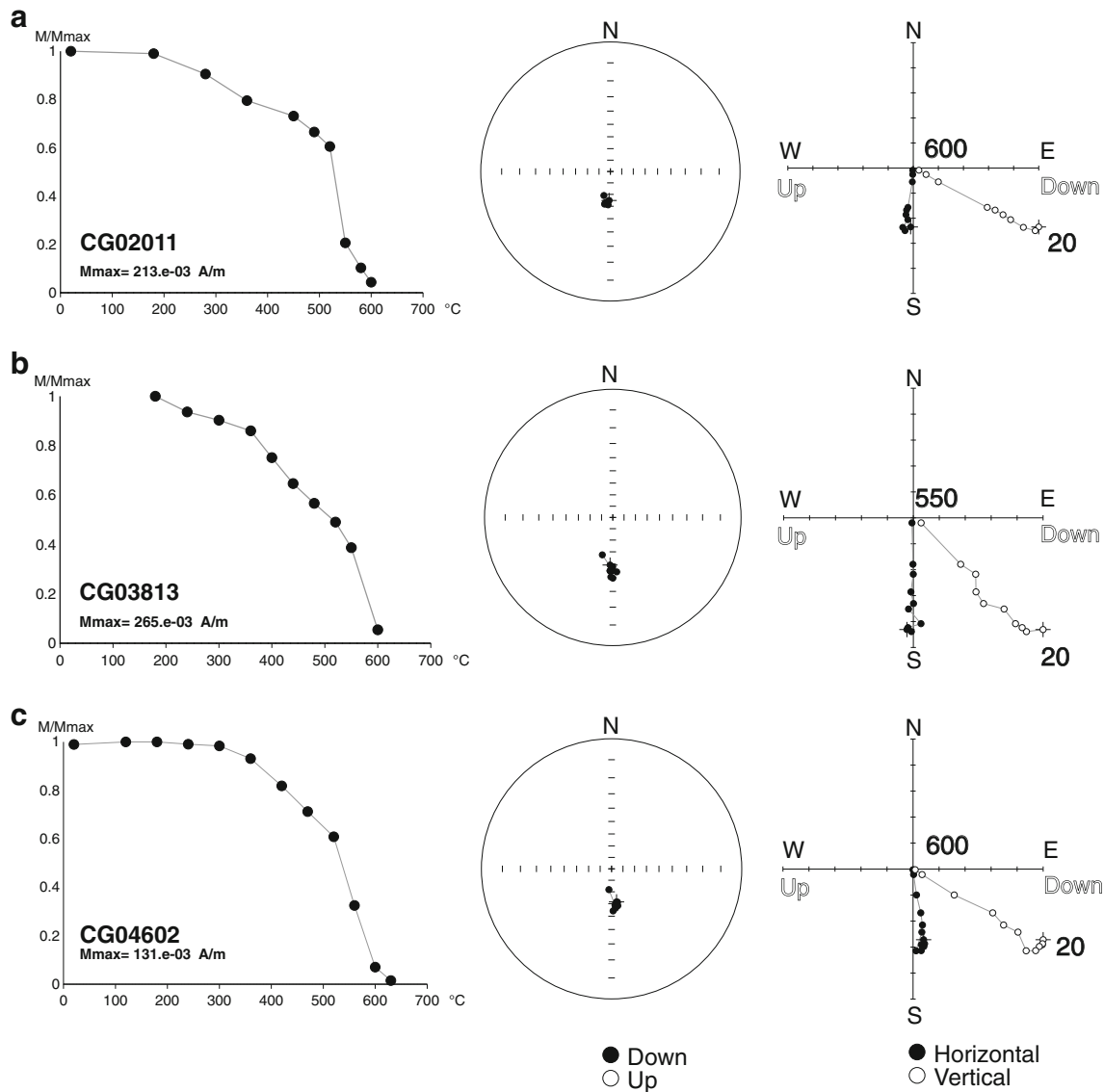
Fig. 10 Representative intensity decay, equal area stereonet, and Z-plots of Cerro Galán ignimbrite TRM analysis. **a**–**c** Single component (class A) demagnetization vectors. Symbols as in Fig. 8. Sample references in "Appendix 2"

part show single component demagnetization vector, completely demagnetized at 600°C and 550°C, respectively. The other three samples show exactly the same behavior at the core and rim, completely demagnetized between 580°C and 600°C with a single component demagnetization vector.

Estimation of the ignimbrites' emplacement temperature

As described above, all the ignimbrites of the Toconquis Group and the Galán ignimbrite, except the Lower Merihuaca unit, show a predominance of class A clasts, with unblocking temperatures ranging mostly between 520° C and 620°C. Lower Merihuaca class B clasts constrain estimates of the emplacement temperature of this unit between 580°C and 610°C.

The temperature estimation at each single site is evaluated on the basis of clast classification. Clasts with VRM are either classified as class A or B on the basis of the behavior at higher demagnetization step, and therefore, we refer to the behavior of the other components to set the emplacement temperature.

In class A clasts (with a single component of magnetization), the magnetization is stable up to the maximum blocking temperature of its magnetic minerals, and its orientation does not change during heating process. This suggests that the clasts were heated to temperatures equal or higher than their maximum blocking temperatures.

Fig. 11 Equal area stereonets of the remanence directions of the Cerro Galán ignimbrite. Symbols as in Fig. 9

Emplacement temperatures that exceed the Curie temperatures of magnetic minerals present in the clasts cannot be defined by paleomagnetic techniques. For this reason, we estimate a minimum emplacement temperature on the basis of the laboratory unblocking temperature T_{ub}, which mirrors the Curie temperature distribution of class A clasts. The fact t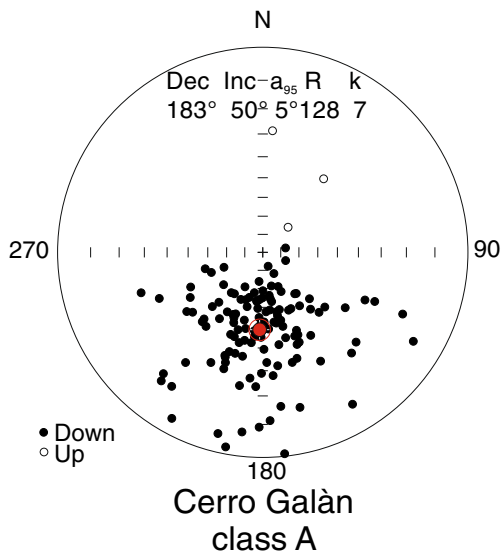hat the clasts locally ripped up from the substrate are also in class A allows us to confirm that they were heated at temperatures higher than Curie temperatures during transport and after emplacement of ignimbrite, something which instead could be questioned for accessory lithics, since they may have been pre-heated within the conduit and may not reflect emplacement temperatures.

For those sites dominantly containing B clasts, the estimation of the emplacement temperature is constrained between the maximum temperature of the LT component and the minimum temperature of the HT component (McClelland and Druitt 1989). In this work, only Lower Merihuaca ignimbrite contains a representative number of class B clasts. Here, the separation of LT and HT components occurs in a very narrow interval, leading us to estimate an emplacement temperature between 580°C and 610°C. In the same site, clasts with higher temperatures belonging to class A were probably heated at vent before being incorporated in the pyroclastic flow, preserving very high temperature at emplacement. In agreement with temperature estimations of the Lower Merihuaca emplacement are those related to magma pre-eruptive temperatures calculated by Folkes et al. (2011b). The authors have estimated pre-eruptive temperatures for all the outcropped ignimbrites (i.e., Cerro Galán, Cueva

Negra and Toconquis Group ignimbrites) applying different geothermometers. They found that the lowest pre-eruptive mean temperatures of Toconquis Group are those estimated for the Lower Merihuaca ignimbrite (e.g., 781± 39°C, hornblende–plagioclase geothermometer), whereas the rest of the ignimbrites have higher temperatures, between 790°C and 820°C.

Cerro Galán ignimbrite is characterized by the prevalence of class A clasts, with a single magnetic component. The frequency distribution of the T_{ub} for all clasts from Cerro Galán ignimbrite is reported in Fig. 12a. The majority of the T_{ub} values (60%) are in the range between 540°C and 580°C, indicating that the main magnetic carrier is magnetite ($T_c = 580$°C) or Ti-magnetite, as the unblocking temperature is not only characteristic of the mineralogy but also of magnetic grain size (not investigated in this study) as shown by magnetic mineralogy analysis. The remaining 40% is equally distributed in the range of 500–540°C and 600–620°C, indicating that the magnetic carriers in these clasts are titanomagnetite and hematite, respectively. We can therefore conclude that Cerro Galán ignimbrite was emplaced at temperature higher than the maximum unblocking temperature T_{ub} of the samples, which is 620°C.

There is no variation of the T_{ub} with distance from the caldera ($R^2 = 0.4$; Fig. 12b). Furthermore, T_{ub} does not vary with lithology, as shown in Fig. 12c. Modal T_{ub} values lie between 540°C and 580°C for all lithologies (in black dacites, all T_{ub} values lie between 540°C and 580°C), except for generic lava clasts (which exclude the plagioclase-phyric dacites), in which the mode of T_{ub} values lies in the 500–540°C interval. As reported in the sampling section, ppd is the most common lithology of the accidental clasts, though it is not encountered in outcrop outside the caldera. It could derive both from proximal lava outflows, ensuring low temperature before ignimbrite emplacement, or possibly from an intracaldera dome or conduit. In this case, the initial temperature of the clasts could have been higher than ambient temperature. This occurrence does not affect the results, however, as the ppd unblocking temperatures and demagnetization vector directions are the same as the other lithologies.

The distribution of minimum emplacement temperatures of the Cerro Galán ignimbrite and Real Grande ignimbrite is shown in Fig. 13a. Site emplacement temperatures are evaluated as the maximum T_{ub} among the measured clasts sampled at each site.

Figure 13b shows T_{ubs} for the Toconquis Group units. Unit emplacement temperatures are defined as the maximum site T_{ub} obtained for the unit, except for Lower Merihuaca where the emplacement temperature (T_e) interval is reported.

Fig. 12 a Frequency histogram of unblocking temperatures (T_{ub}) for CGI. Most of the analyzed samples show unblocking temperatures between 540°C and 580°C; **b** unblocking temperatures variation with distance; the best fit linear regression gives a slope of 1.2, but the values scatter is wide (r^2 varies between 0 and 1 for individual points), the correlation coefficient is low (r varies between 0 and 1 for individual points); and statistical significance is high ($p \ll 0.1\%$); **c** unblocking temperatures variation for the most representative lithologies. *ppd* plagioclase-phyric dacite, *bppd* black plagioclase-phyric dacite, *mvo* metavolcanic Ordovician, *ms* mica-schist
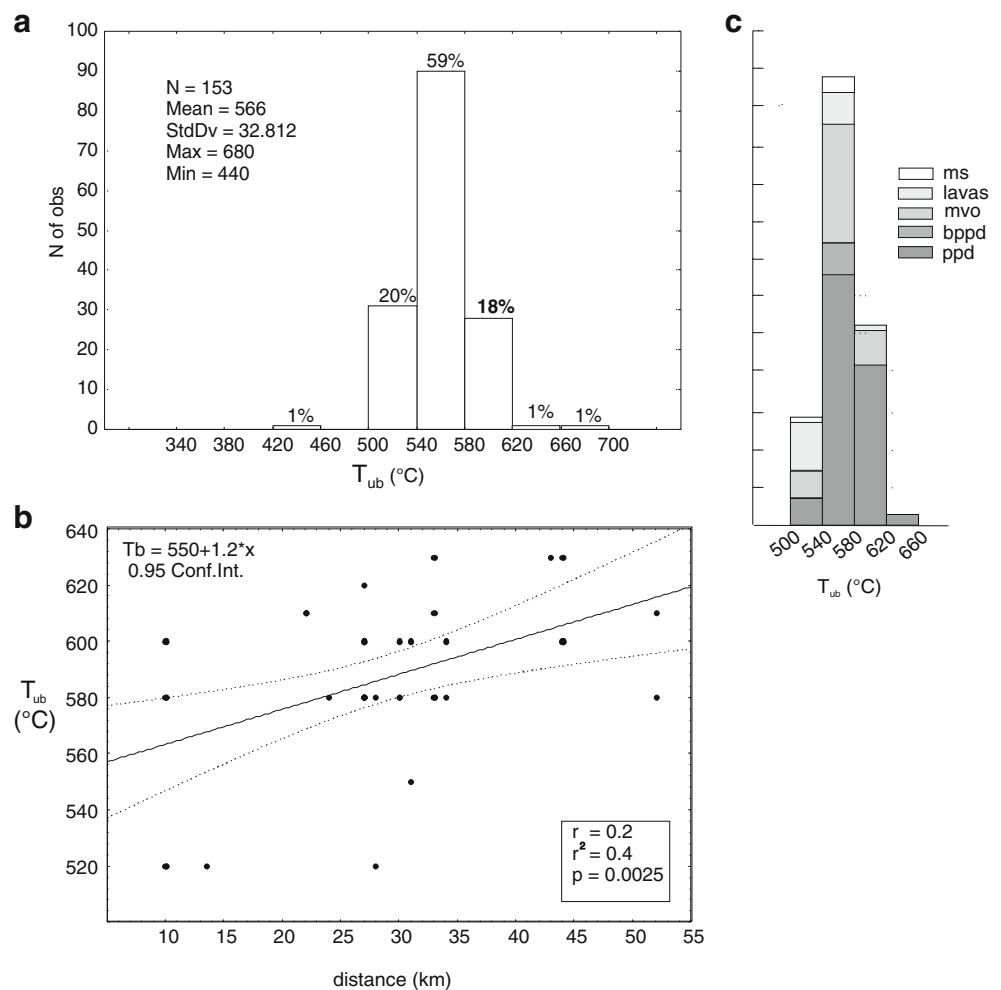
Implications on emplacement mechanism of the Cerro Galán and Toconquis Group ignimbrites

The results of the TRM analysis carried out on the Cerro Galán and Toconquis Group ignimbrites revealed emplacement temperatures higher than 600°C in most cases. High emplacement temperatures in pyroclastic flow deposits have been found worldwide, both by means of direct measurement and indirect analysis. In Guadeloupe, in the 37-ka *nuée ardente* of La Créte à Bambous, Zlotnicki et al. (1984) found emplacement temperatures up to 530°C. For the 1993 eruption of Volcán de Láscar in Chile, Paterson et al. (2010) retrieved emplacement temperatures of the pyroclastic flow exceeding the Curie temperature of magnetic minerals (>400°C) up to 8.5 km from the source. At Soufriere Hills, Montserrat, Calder et al. (1999) directly measured temperatures up to 650°C, while Scott et al. (2008) found temperatures in the range of 400–610°C by the analysis of vitrinite reflectance. Direct measurements of Mt. St. Helens 1980 deposits (Banks and Hoblitt 1981) indicated a settling temperature of the 22 July eruption of

705°C, 6.9 km from the vent. Moreover, numerical simulations of small to large volume pyroclastic flows indicate that the deposits may retain high temperatures (Giordano and Dobran 1994; Todesco et al. 2006).

TRM data constrain the thermal structure of the Cerro Galán ignimbrite immediately after deposition at $T > 580$–620°C, along the entire extent of the preserved deposit (maximum distance investigated is 52 km from caldera rim) and also along vertical sections (max 60 m thick). Temperature estimations for Toconquis Group ignimbrites give the same indications, except for Lower Merihuaca ignimbrite where more precise and lower (580–610°C) emplacement temperatures are estimated.

In addition, the TRM analysis of Cerro Galán specimens obtained from the core and the rim of a single large lithic clast shows that the thermal behavior is homogeneous throughout the clast. Using the heat transfer model of Carslaw and Jaeger (1959), Bardot (2000) estimated that clasts sized between 2 and 10 cm, initially at ambient temperature, will reach thermal equilibrium with the medium after 10^2–10^4 s, respectively, i.e., within hours.
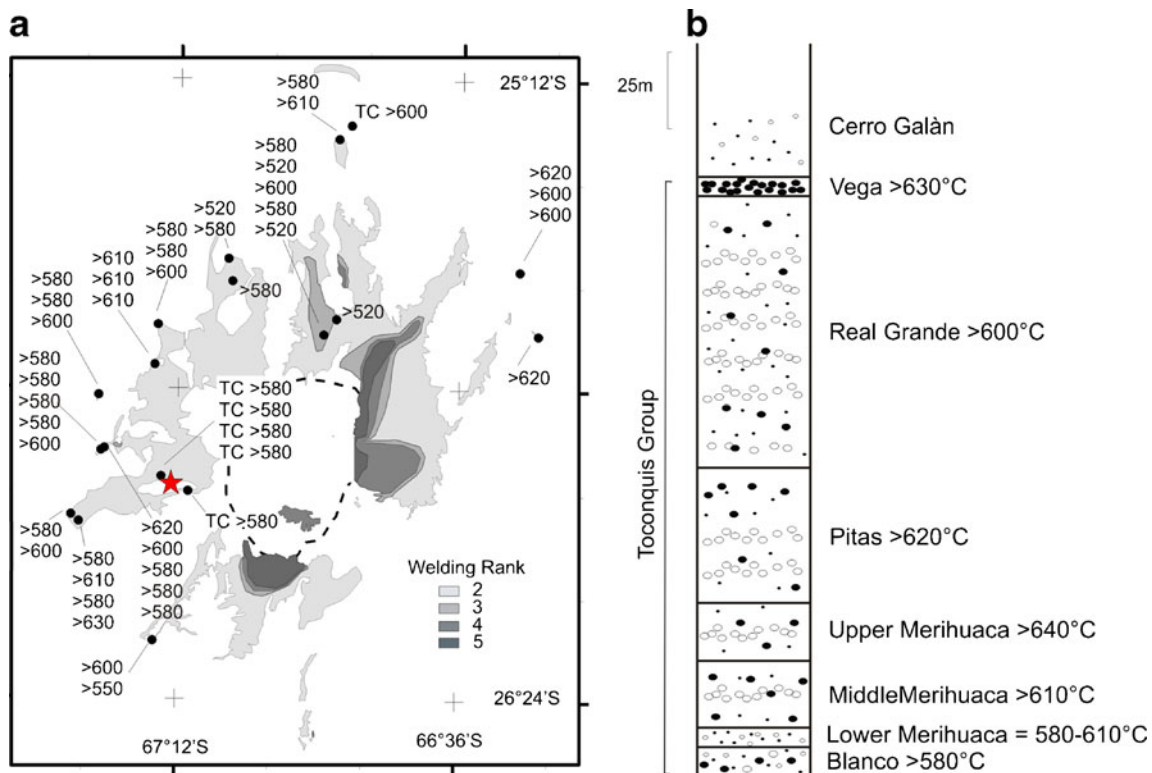
Fig. 13 a Site unblocking temperature (T_{ub}) areal distribution for Cerro Galán (*CG*) ignimbrite and Toconquis Group (*TC*) ignimbrite (Real Grande ignimbrite). Sites ID as in Fig. 4. Welding ranks for Cerro Galán ignimbrite (ranks II–V) are represented in four *gray levels*, according to the ranking scheme of Quane and Russell (2005).

Note as the highest ranking values (IV–V) are limited to the eastern side of the caldera. **b** Site T_{ub} results for the Toconquis Group ignimbrites at Rio Las Pitas, Vega Real Grande section (*red star* in Fig. 13a)

Minimum estimates of cooling rate prior to emplacement reported in Wright et al. (2011a) vary between 3×10^{-3} and 8.5×10^{-2}°C/min, based on the lack of welding textures. Since the analyzed clasts between 2 and 10 cm in diameter are completely remagnetized in the Cerro Galán ignimbrite, we can argue that the minimum emplacement temperature required to remagnetize the clast at the cooling rates calculated by Wright et al. (2011a) varies between 621° and 635°C.

We can constrain the T dissipation path of the Cerro Galán eruption first assuming that the initial temperature was the magmatic temperature (T_m), which is inferred by Fe–Ti oxide geothermometry to be maximum of 790°C (cf. Folkes et al. 2011b). Adopting this estimated temperature as the T_m at the fragmentation level, the maximum temperature drop from fragmentation to emplacement is ~200°C. Furthermore, we can use the areal distribution of the partial welding in the CGI (Fig. 14) to define the distance at which the deposit temperature crossed the glass transition temperature (T_g) prior to emplacement. The welding ranks were determined on the basis of field occurrences, following the Quane and Russel (2005) classification. Thin section analysis carried out on 35 matrix cores did not allow a

ranking attribution, since the extensive recrystallization obliterated the glassy shards structures in most of the samples. The majority of the sites are rank II, while the maximum welding encountered is rank V, since some vesiculation could be still detected in some *fiamme*. Figure 13 shows how welding is unevenly distributed in the CGI, being more extensively present east of the caldera compared to the west, north, and south. The maximum distance to which the welding degree of the deposit can be ranked higher than rank II is 23 km, and this defines, given the compositional and loading characteristics, an emplacement temperature close to T_g. The maximum T_g calculated for an anhydrous rhyodacitic magma is ~780°C, decreasing to less than 550°C with 2% of dissolved H_2O and decreasing also at increasing strain rates (Giordano et al. 2006).

Figure 14 summarizes the reconstructed thermal structure of the CGI and the implications of this thermal structure for the mechanism of transport and deposition of the CGI pyroclastic flows. Based on high temperature estimates throughout the ignimbrite, we infer that the CGI pyroclastic flow was conservative in terms of temperature dissipation.

Cooling of the pyroclastic flow, containing a mixture of gas, lithics, and juvenile fragments, is related to several
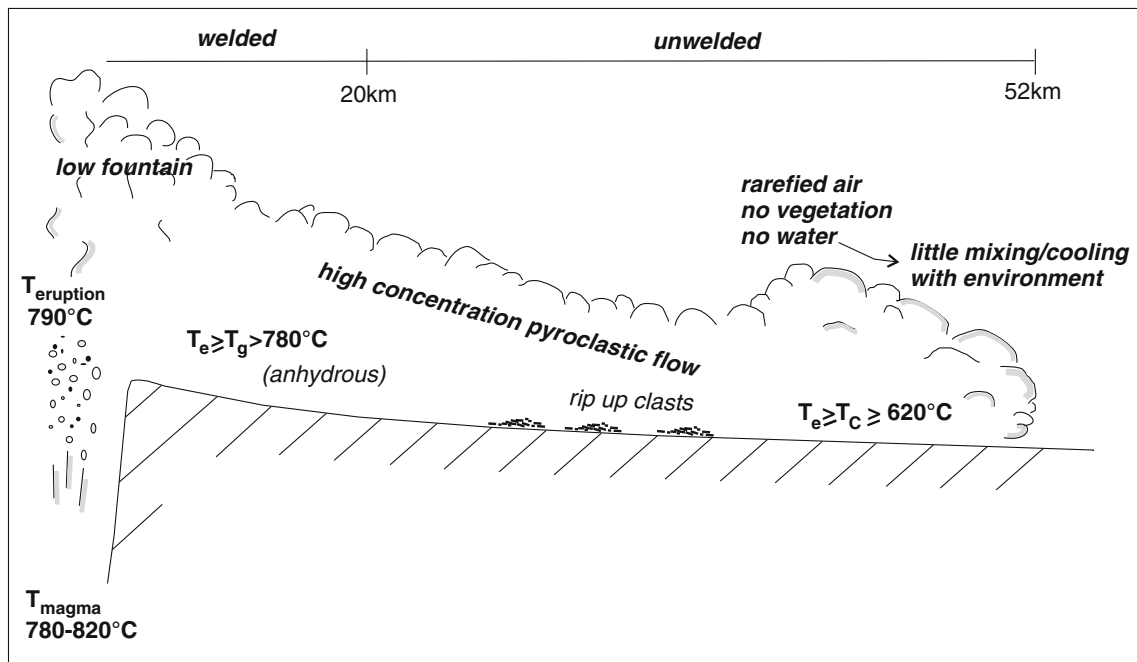
Fig. 14 Schematic ignimbrite temperature profile from the vent to distal sites

processes that include convective heat transport, radiative heat transfer, gas adiabatic expansion, and heat conduction (e.g., Bardot 2000 and references therein). Cooling by adiabatic decompression is usually relatively small and estimated to be about 90°C for the 1.8-ka Taupo ignimbrite, produced after the collapse of a plinian eruption column (McClelland et al. 2004 and references within). Air ingestion during an explosive eruption mainly occurs within the sustained column phase and, to a minor extent, during the collapsing phase, with the area most subject to subsequent air entrainment being the flow front (Cas and Wright 1987). In the CGI case, the absence of a basal fall deposit excludes the occurrence of an early plinian phase and indicates either boiling-over processes or low fountaining to produce pyroclastic flows (Cas et al. 2011). Both eruptive conditions limit heat loss above the vent region. Consequently, we take the estimate at Taupo as an absolute maximum for temperature loss accompanying decompression during the Cerro Galán eruptions.

Perhaps more significantly, the amount of convective, radiative, and conductive heat dissipation is largely a function of the density and hence particle concentration of the flow. Convective and radiative heat loss can be considered as a particle-surface phenomenon (Martì et al. 1991); therefore, the contribution of convective and radiative heat transfer increases as the dilution of the density current increases. In contrast, heat conduction is a more efficient heat transfer mechanism in dense flows and in the presence of accidental clasts >1 cm in size (Bardot 2000).

The process of convective heat transfer in a pyroclastic flow depends on the temperature disequilibria between the pyroclasts, the lithics, and the gas (T_{gas}) (Bardot 2000). The T_{gas} drives the cooling of the pyroclastic flow, as gases able to convectively admix with ambient air cool faster than pyroclasts. The T_{gas} decreases progressively from the conduit/vent into the uprising jet and down to the collapsing ground-hugging flow. T_{gas} further decreases with increased air entrainment (Todesco et al. 2006) or interaction with water and incorporation of vegetation and cold accidental lithic clasts (McClelland et al. 2004; Cioni et al. 2004).

The desert environment of the Puna Plateau, characterized by 5–10% humidity and 65 mm of precipitation on annual average (Bianchi and Yañez 1992; Arias and Bianchi, 1996), makes it extremely unlikely that significant incorporation of surface water or vegetation took place, further reducing the chances of an effective bulk mixing of the pyroclastic flow with the environment. Additionally, McClelland et al. (2004) inferred at Taupo that the incorporation of 16% in weight of lithics at the source, with temperatures of 20°C and heat capacities similar to the juvenile material, would reduce the temperature of the pyroclastic flow from the magmatic temperature by 210°C. In the Cerro Galán ignimbrite, the lithic content is generally very low (<1–5%) and therefore cannot account for significant cooling.

The low degree of heat loss along the pyroclastic flow path is evaluated also in the context of the altitude of the area, ranging between ~3,000 and ~5,000 m a.s.l. At these elevations, the atmosphere is more rarefied and is likely to offer lower frictional resistance on the spreading pyroclastic flow, effectively lowering the extent of the mixing and air entrainment. Air density, without taking into account air

moisture (almost negligible in the Puna Plateau), is about 0.6 kg/m^3 at 5,000 m a.s.l., i.e., a half of that at sea level.

Air entrainment therefore plays a major role in determining the emplacement temperature in distal facies. As widely recognized (e.g., Cas and Wright 1987), air entrainment occurs mostly in the eruption column and subsequently at the head and in the body of the pyroclastic flow, where turbulent eddies may incorporate overlying air (Bursik and Woods 1996). In the Cerro Galán ignimbrite, a low eruption column inhibited a significant heat exchange at that stage. Moreover, the absence of veneer facies on ridges indicates a low level of dilution and low amount of air entrainment in the body. Point counts of co-existing ash matrix glass and pumice glass (Folkes et al. 2011a) showed that at distal localities of the ignimbrite outflow sheet, there is a depletion in matrix ash of 17–34%. The authors adopt a conservative value of 30% in ash depletion to evaluate the volume of the elutriated material. On the other hand, the matrix crystal content (35–45%, Folkes et al. 2011a) is comparable to the pumices' crystal content (35–49% in gray pumices, 44–57% in white pumices, Wright et al. 2011b) indicating a very low degree of ash depletion, which in turns indicates a low level of air ingestion.

In addition, heat dissipation depends on the bulk degree of fragmentation and overall grain size. The larger the proportion of fine-grained particles, the easier and faster the heat exchange with the fluid (gas/atmosphere) environment during flow (Cas and Wright 1987). The CGI ignimbrite is a mostly fine-grained deposit (Wright et al. 2011b). The fine-grained nature of the particle population would provide more favorable conditions for an efficient convective and radiative heat exchange with the environment. The low degree of cooling experienced by the CGI (≤200°C as said above) cannot therefore be related to the grain size of the pyroclasts and must be interpreted instead as a result of the high particle concentration and limited interaction with the external environment.

In summary, the consistent high emplacement temperature of the flow, both along section and at increasing distance from the caldera, involving a maximum temperature drop from magmatic temperature of less than 200°C, is indicative of a thermally conservative flow. Temperature conservation can be attributed mainly to the high particle concentration in the flow, which had very limited interaction with the environment as indicated also by the high fine particles content. Low fountaining, deduced from the absence of a basal fall deposit, inhibited the main process for cooling, i.e., air entrainment in the eruption column; the density of the flow itself further inhibited flow-head and body air entrainment during flow emplacement, as also supported by the lack of veneer facies deposits. Lithics in the flow did not act as a cooling factor, as lithic content is very low. Water and vegetation played no role, or a very small one at local scale, due to the extremely arid environment.

Conclusions

We estimated minimum emplacement temperatures on the basis of paleomagnetic analysis of lithic clasts embedded in the ignimbrites of the Cerro Galán volcanic system. The main results are:

1. The main magnetic carriers in accidental lithic clasts in the Cerro Galán ignimbrites are magnetite and to a minor extent hematite, maghemite, and titanomagnetite. No significant mineralogical alteration occurred during laboratory heating procedures, confirming the reliability of the TRM analysis;
2. Two classes of paleomagnetic behavior were identified by TRM analysis: clasts with a single component demagnetization vector (class A) and clasts with two demagnetization vector components (class B).
3. Unblocking temperatures T_{ub} were estimated for each clast and verified in the range 520–620°C; where T_{ub} ~580°C, the magnetization is carried by magnetite; when T_{ub} is ~620°C, then it is carried by hematite.
4. The Cerro Galán ignimbrite was emplaced at temperatures equal or higher than 620°C, even at distal sites. Similar high temperatures characterized the units of the Toconquis Group, with the emplacement temperature determined at 580–610°C for the Lower Merihuaca ignimbrite and equal to or higher than 620°C for the other ignimbrites of the group.

The large volume Cerro Galán ignimbrite is a very conservative ignimbrite in terms of temperature. A maximum temperature drop of 200°C can be accounted for between fragmentation and emplacement. Such conditions can be explained by a combination of effects, in part related to the low accessory/accidental lithic content, in part to low-height fountaining at vent(s), and in part to the high particle concentration of the pyroclastic flow(s), with minimal air, water, and vegetation entrainment along the flow paths, favored by the particularly high altitude and desert conditions of the Puna Plateau. Such conditions could facilitate low bulk turbulence level of the pyroclastic flow(s), in agreement with the field evidence of the strong topographic control on the Cerro Galán Ignimbrite and the absence of veneer facies.

Appendix 1

Table 5 Toconquis Group samples TRM results

Unit	Sample	Lithology	Single component	2 components		Class	T_{ub} (°C)
				LT	HT		
Blanco	TC02111	ppd	n			A	>580
	TC02112	ppd	n			A	>580
	TC02113	ppd	n			A	>580
	TC02114A	ppd	n			A	>580
	TC02114B	ppd	n			A	>580
	TC02115	ppd	n			A	>580
	TC02116	ppd	n			A	>580
Lower Merihuaca	TC02121	ppd		n	rand	B	580–600
	TC02122	ppd	n			A	>630
	TC02123	ppd	n			A	>580
	TC02124	ppd	n			A	>580
	TC02125	ppd	n			A	>630
	TC02126	ppd		n	rand	B	580–600
	TC07301	ppd		n	rand	B	590–610
	TC07302	ppd	n			A	>530
	TC07303	ppd	n			A	>560
	TC07305	ms		n	rand	B	590–610
	TC07306	ppd		n	rand	B	590–610
	TC07307	ppd		n	rand	B	590–610
	TC07308	ppd	n			A	>560
	TC07309	ppd		n	rand	B	590–610
	TC07310	ppd	n			A	>610
	TC07311	ppd		n	rand	B	590–610
	TC01611	Lava	n			A	>580
	TC01612	Lava	n			A	>580
	TC01614	Lava	n			A	>580
	TC01615	Lava	n			A	>580
	TC01616	ppd	n			A	>580
	TC01621	Lava	n			A	>580
	TC01625	Lava	r			A	>580
	TC02131	ppd	\	\	\	\	\
Middle Merihuaca	TC02132	ppd		n	rand	B	360–480
	TC02133	ppd	n			A	>580
	TC02134	ppd	n			A	>600
	TC02135	ppd	n			A	>580
	TC02136	ppd	n			A	>580
	TC02211		n			A	>600
	TC02213	ppd	n			A	>580
	TC02214	ppd	n			A	>580
	TC07401	bppd	n			A	>560
	TC07402	ig	n			A	>560
	TC07403	ppd	n			A	>610
	TC07404	ppd	n			A	>610

Table 5 (continued)

Unit	Sample	Lithology	Single component	2 components		Class	T_{ub} (°C)
				LT	HT		
	TC07405	ppd	n			A	>610
	TC07406	ppd	n			A	>610
	TC07407	ppd	n			A	>610
	TC07408	ig	n			A	>590
	TC07409	ig	n			A	>590
	TC07410	ppd	n			A	>610
Upper Merihuaca	TC02141	\	\	\	\	\	\
	TC02142	Rhyolite	r			A	>480
	TC02143	ppd	r			A	>580
	TC02146	ppd	r			A	>580
	TC02222	ppd	r			A	>620
	TC02223	ppd	r			A	>580
	TC02225	ppd	r			A	>580
	TC02226	ppd	\	\	\	\	\
	TC02313	ppd	r			A	>620
	TC02314	ppd	r			A	>580
	TC02315	ppd	r			A	>580
	TC02316	ppd	\	\	\	\	\
Upper Merihuaca	TC07501	ppd	n			A	>610
	TC07502			r	rand	B	530–560
	TC07503	mvo	\	\	\	\	\
	TC07504	mvo	r			A	>340
	TC07505	mvo	r			A	>460
	TC07506		r			A	>590
	TC07507		r			A	>420
	TC07508		r			A	>590
Pitas	TC02151		n			A	>600
	TC02152	ppd	n			A	>600
	TC02153	ppd	n			A	>580
	TC02154		n			A	>600
	TC02155		n			A	>600
	TC02156		n			A	>580
	TC02411	ppd	n			A	>620
	TC02412	ppd	n			A	>620
	TC02413	ppd	n			A	>580
	TC02414	ppd	n			A	>580
	TC02415	ppd	n			A	>580
	TC02416		n			A	>580
	TC02511	ppd	r			A	>620
	TC02512		n			A	>580
	TC02513	ppd	n			A	>600
	TC02516		n			A	>580
	TC07701	ppd	n			A	>610
	TC07702	ppd	n			A	>590

Table 5 (continued)

Unit	Sample	Lithology	Single component	2 components		Class	T_{ub} (°C)
				LT	HT		
	TC07703	ppd	n			A	>590
	TC07704	ppd	n			A	>590
	TC07705	ppd	n			A	>560
	TC07706	ppd	n			A	>590
	TC07707	ppd	n			A	>560
	TC07708	ppd	n			A	>590
Pitas	TC07801	ppd	n			A	>610
Real Grande	TC01712	ppd	n			A	>580
	TC01722	ppd	n			A	>580
	TC01921	fms	n			A	>580
	TC01925	ppd	n			A	>580
	TC02611	ppd	n			A	>480
	TC02612	ppd	n			A	>580
	TC02613	ppd	n			A	>580
	TC02621	ppd	n			A	>600
	TC02622	ppd	n			A	>600
	TC02623	ppd	n			A	>520
	TC02624	ppd	n			A	>620
	TC02625	ppd	n			A	>600
	TC02626	ppd	n			A	>580
	TC02631	ppd	r			A	>580
	TC02632	ppd	n			A	>580
	TC02633	ppd	n			A	>600
	TC03021	ppd	n			A	>580
	TC03026	ppd	n			A	>580
	TC03031	ppd	n			A	>580
	TC03052	ppd	n			A	>580
	TC06201	ms	n			A	>600
	TC06202	ppd	n			A	>600
	TC06204	ppd	n			A	>630
	TC06205	fms	n			A	>630
	TC06207	ppd	n			A	>600
	TC06208	ppd	n			A	>600
Vega	TC02641	ppd	r			A	>520
	TC02642	ppd	r			A	>520
	TC02643		r			A	>560
	TC02644		r			A	>530
	TC02645		r			A	>530

Sample ID: The first four numbers correspond to the site number (cf. Tables 2 and 3); clast lithology (ppd, bppd, ms, mvo, fms, ig, amph, qz, qbs, gms, gr), magnetic polarity of single component (n, r), two (LT and HT) magnetic components (n, r, rand), clast classification and estimated blocking temperature

ppd phyric-plagioclase dacite, *bppd* black phyric-plagioclase dacite, *ms* metasediment, *mvo* metavolcanic, *fms* fine mica shist, *ig* older ignimbrite, *amph* amphibolite, *qz* quartzite, *qbs* quartz-biotite schist, *gms* garnet mica-schist, *gr* granite, *n* normal, *r* reverse, *rand* random

Appendix 2

Table 6 Cerro Galán samples TRM results

Sample	Lithology	Single component	2 components		Class	T_{ub} (°C)
			LT	HT		
CG00121	ppd	r			A	>610
CG00122	ppd	r			A	>580
CG00131	ppd	r			A	>580
CG00132	ppd	r			A	>580
CG00133	ppd	r			A	>580
CG00211	ppd	r			A	>520
CG00312	Lava	r			A	>520
CG00313	Lava	r			A	>520
CG00314	Lava	r			A	>520
CG00315	mvo	r			A	>520
CG00316	Lava	r			A	>520
CG00321	mvo	r			A	>580
CG00322	mvo	r			A	>520
CG00323	Lava	r			A	>520
CG00324	Lava	r			A	>520
CG00331	Lava	r			A	>520
CG00332	Lava	r			A	>520
CG00333	Lava	r			A	>520
CG00334	Lava	r			A	>520
CG00335	Lava	r			A	>600
CG00336	Lava	r			A	>520
CG00342	amph	r			A	>520
CG00343	\	r			A	>520
CG00344	amph	r			A	>520
CG00351	Lava	r			A	>520
CG00352	mvo	\	\	\	\	\
CG00353	Lava	r			A	>520
CG00415	Lava	r			A	>580
CG00422	ms	r			A	>520
CG00511	qbs	r			A	>580
CG00514	ms	r			A	>580
CG00515	mvo	r			A	>580
CG02011	Lava	r			A	>600
CG02012	mvo	r			A	>600
CG02012B	mvo	\	\	\	\	\
CG02013	mvo	\	\	\	\	\
CG02014A	qz	r			A	>550
CG02014B	qz	\	\	\	\	\
CG02015	mvo	\	\	\	\	\
CG02016	mvo	r			A	>550
CG02017	mvo	r			A	>600
CG02021	mvo	r			A	>550
CG02022	mvo	r			A	>580

Table 6 (continued)

Sample	Lithology	Single component	2 components		Class	T_{ub} (°C)
			LT	HT		
CG02024	fms	r			A	>440
CG02025	fms	r			A	>580
CG02026	mvo	r			A	>580
CG02031	mvo	r			A	>580
CG02032	\	r			A	>580
CG02034	\	r			A	>580
CG02035	qz	n			A	>550
CG02036A	\	r			A	>580
CG02036B	\	r			A	>580
CG02037	mvo	r			A	>580
CG02039	mvo	r			A	>580
CG02041	ms	n			A	>580
CG02042	ms	r			A	>580
CG02043	ms	r			A	>520
CG02051	mvo	/	/	/	/	/
CG02052	mvo	r			A	>580
CG02053	mvo	r			A	>550
CG02711	mvo	r			A	>580
CG02712	mvo	r			A	>580
CG02713	mvo	r			A	>550
CG02714	mvo	r			A	>580
CG02721	mvo	r			A	>550
CG02723	mvo	r			A	>600
CG02724	mvo	r			A	>600
CG02725	mvo	r			A	>580
CG02811	fms	r			A	>520
CG02812	mvo	r			A	>580
CG02813	mvo	r			A	>620
CG02814	mvo	r			A	>550
CG02815A	mvo	r			A	>600
CG02815B	mvo	r			A	>600
CG02816	mvo	r			A	>600
CG02821	fms	\	\	\	\	\
CG02822	mvo	r			A	>580
CG02823	fms	r			A	>520
CG02824	mvo	r			A	>520
CG02825	mvo	r			A	>520
CG02826	mvo	r			A	>580
CG02831	mvo	\	\	\	\	\
CG02832	mvo	\	\	\	\	\
CG02833	mvo	\	\	\	\	\
CG02834	fms	\	\	\	\	\
CG02835	mvo	\	\	\	\	\
CG02836	ppd	r			A	>580
CG02841	ig	r			A	>580
CG02842	mvo	r			A	>580
CG02843	mvo	n			A	>580

Table 6 (continued)

Sample	Lithology	Single component	2 components		Class	T_{ub} (°C)
			LT	HT		
CG02852	mvo	r			A	>520
CG02853	\	r			A	>580
CG02854	\	\	\	\	\	\
CG02855	\	\	\	\	\	\
CG02856	\	r			A	>600
CG03421	ppd	\	\	\	\	\
CG03422	ppd	\	\	\	\	\
CG03423	ppd	\	\	\	\	\
CG03424	ppd	\	\	\	\	\
CG03425	bppd	r			A	>580
CG03426	mvo	r			A	>600
CG03431	Lava	r			A	>580
CG03432	ppd	r			A	>580
CG03433	Lava	r			A	>580
CG03435	\	r			A	>520
CG03436	\	\	\	\	\	\
CG03441	ppd	r			A	>580
CG03442	ppd	r			A	>580
CG03443	ppd	r			A	>580
CG03444	ppd	r			A	>550
CG03511	mvo	r			A	>580
CG03513	ppd	r			A	>610
CG03514	ppd	r			A	>610
CG03515	mvo	r			A	>580
CG03516	ppd	r			A	>610
CG03521	ppd	r			A	>580
CG03522	ppd	r			A	>610
CG03523	ppd	r			A	>580
CG03524	ppd	r			A	>580
CG03525	ppd	r			A	>580
CG03526	ppd	r			A	>550
CG03531	ppd	r			A	>610
CG03532	ppd	r			A	>610
CG03533	ppd	r			A	>580
CG03711	mvo	r			A	>550
CG03712	mvo	r			A	>580
CG03713	mvo	r			A	>550
CG03716	mvo	r			A	>550
CG03721	mvo	r			A	>550
CG03722	ppd	r			A	>610
CG03731	ppd	r			A	>520
CG03732	ppd	r			A	>580
CG03733	ppd	r			A	>520
CG03734	ppd	\	\	\	\	\
CG03735	ppd	r			A	>550
CG03741	mvo	r			A	>630
CG03742	mvo	\	\	\	\	\

Table 6 (continued)

Sample	Lithology	Single component	2 components		Class	T_{ub} (°C)
			LT	HT		
CG03743	mvo	\	\	\	\	\
CG03744	mvo	r			A	>580
CG03745	mvo	\	\	\	\	\
CG03811	gms	r			A	>600
CG03812	gms	r			A	>550
CG03813	ppd	r			A	>550
CG03814	gms	r			A	>600
CG03821	\	r			A	>550
CG03822	qbs	\	\	\	\	\
CG03823	qbs	r			A	>550
CG03824	qbs	r			A	>550
CG04201	ms				A	>580
CG04205	gr	\	\	\	\	\
CG04206	gr	r			A	>630
CG04207	gr	r			A	>650
CG04301	gr	r			A	>560
CG04302	gr	r			A	>560
CG04303	gr	r			A	>560
CG04304	gr	r			A	>560
CG04305	gr	r			A	>600
CG04308	gr	\	\	\	\	\
CG04401	ppd	r			A	>560
CG04402	ppd	r			A	>560
CG04404	ppd	r			A	>600
CG04405	ppd	r			A	>600
CG04406	ppd	r			A	>560
CG04407	ppd	r			A	>560
CG04409	Spatterlike	r			A	>560
CG04410	ppd	r			A	>600
CG04601	fms	r			A	>600
CG04602	fms	r			A	>600
CG04603	ppd	r			A	>560
CG06601	bppd	r			A	>550
CG06602	bppd	r			A	>550
CG06603	bppd	r			A	>550
CG06604	bppd	r			A	>550
CG06606	bppd	r			A	>550
CG06607	bppd	r			A	>550
CG06608	bppd	r			A	>600

Fields as in "Appendix 1"

References

Aramaki S, Akimoto S (1957) Temperature estimation of pyroclastic deposits by natural remanent magnetism. Am J Sci 255:619–627

Arias M, Bianchi AR (1996) Estadisticas Climatologicas de la provincia de Salta. INTA, Salta

Banks NG, Hoblitt RP (1981) Summary of temperature studies on 1980 deposits. In: Lipman PW, Mullineaux DR (eds) The 1980 eruptions of Mount St. Helens. USGS Prof Paper 1250. USGS, Washington, DC, pp 295–314

Bardot L (2000) Emplacement temperature determinations of proximal pyroclastic deposits on Santorini, Greece, and their implications. Bull Volcanol 61:450–467

Bardot L, McClelland E (2000) The reliability of emplacement temperature estimates using paleomagnetic methods: a case study from Santorini, Greece. Geophys J Int 143(1):39–51

Bianchi R, Yañez CE (1992) Las precipitaciones en el Noroeste Argentino, IIth edn. INTA-Estación Experimental Agropecuaria Salta, Salta

Branney MJ, Kokelaar BP (2002) Pyroclastic density currents and the sedimentation of ignimbrites. Mem Geol Soc Lond 27:143

Bursik MI, Woods AW (1996) The dynamics and thermodynamics of large ash flows. Bull Volcanol 58:175–193

Calder ES, Cole PD, Dade WB, Druitt TH, Hoblitt R, Huppaert HE, Ritchie L, Spark RSJ, Young SR (1999) Mobility of pyroclastic flows and surges at the Soufriere Hills, Montserrat. Geophys Res Lett 26:537–540

Carslaw HS, Jaeger JC (1959) Conduction of heat in solids. Oxford University Press, Oxford

Cas RAF, Wright JV (1987) Volcanic succession, modern and ancient. Chapman and Hall, London

Cas RAF, Wright HMN, Lesti C, Porreca M, Folkes C, Giordano G, Viramonte J (2011) The flow dynamics of an extremely large volume pyroclastic flow, the 2.08 Ma Cerro Galán Ignimbrite, NW Argentina, and comparison with other flow types. In: Cas RAF, Cashman K (eds) The Cerro Galán ignimbrite and Caldera: characteristics and origins of a very large volume ignimbrite and its magma system. Bull Volcanol (in press)

Cioni R, Gurioli L, Lanza R, Zanella E (2004) Temperature of the A. D. 79 pyroclastic density current deposits (Vesuvius, Italy). J Geophys Res 109:B02207. doi:10.1029/2002JB002251

Chadima M, Hrouda F (2006) Remasoft 3.0 a user-friendly paleomagnetic data browser and analyzer. Travaux Géophysiques 27:20–21

Coira B, Kay SM, Viramonte J (1993) Upper Cenozoic magmatic evolution of the Argentine Puna—a model for changing subduction geometry. Internat Geol Rev 35:677–720

Dunlop DJ, Özdemir Ö (1997) Rock magnetism, fundamentals and frontiers. Cambridge University Press, Cambridge

Fisher RA (1953) Dispersion on a sphere. Proc Roy Soc London 21A:295–305

Folkes CB, Wright HM, Cas RAF, de Silva SL, Lesti C, Viramonte JG (2011a) A re-appraisal of the stratigraphy and volcanology of the Cerro Galán volcanic system, NW Argentina. In: Cas RAF, Cashman K (eds) The Cerro Galan Ignimbrite and Caldera: characteristics and origins of a very large volume ignimbrite and its magma system. Bull Volcanol. doi:10.1007/s00445-011-0459-y

Folkes CB, de Silva SL, Wright HM, Cas RAF (2011b) Geochemical homogeneity of a long-lived, large silicic system; evidence from the Cerro Galan caldera, NW Argentina. In: Cas RAF, Cashman K (eds) The Cerro Galan Ignimbrite and Caldera: characteristics and origins of a very large volume ignimbrite and its magma system. Bull Volcanol. doi:10.1007/s00445-011-0511-y

Francis PW, O'Callaghan LJ, Kretschmar GA, Thorpe RS, Sparks RSJ, Page RN, de Barrio RE, Gillou G, Gonzalez OE (1983) The Cerro Galan ignimbrite. Nature 301:51–53

Freundt A (1998) Formation of high grade ignimbrites. Part II. A pyroclastic suspension current model with implications for low grade ignimbrites. Bull Volcanol 60:545–567

Gonzalez OE (1984) La ignimbritas de "Ojo de Ratones" y sus relaciones regionales, provincia de Salta. In Noveno Congreso Geologico Argentino, Actas I, pp 206–220

Giordano D, Mangiacapra A, Potuzák M, Russell JK, Romano C, Dingwell DB, Di Muro A (2006) An expanded non-Arrhenian model for silicate melt viscosity: a treatment for metaluminous, peraluminous and peralkaline liquids. Chem Geol 229:42–56

Giordano G, Dobran F (1994) Computer simulations of the Tuscolano Artemisio's second pyroclastic flow unit (Alban Hills, Latium, Italy). J Volcanol Geotherm Res 61:69–94

Gradstein F, Ogg J, Smith A (2004) A geologic time scale. Cambridge University Press, Cambridge, p 589

Gurioli L, Pareschi MT, Zanella E, Lanza R, Deluca E, Bisson M (2005) Interaction of pyroclastic density currents with human settlements: evidence from ancient Pompeii. Geology 33(6):441–444

Hoblitt RP, Kellogg KS (1979) Emplacement temperatures of unsorted and unstratified deposits of volcanic rock debris as determined by paleomagnetic techniques. Geol Soc Am Bull Part I 90:633–642

Kay SM, Coira B, Mpodozis C (2008) Field trip guide: Neogene evolution of the central Andean Puna plateau and southern Central Volcanic Zone. Geol Soc of America, fl d013-05:119–181

Kay SM, Coira B, Wörner G, Kay RW, Singer BS (2011) Geochemical, isotopic and single crystal 40Ar/39Ar age constraints on the evolution of the Cerro Galán ignimbrites. In: Cas RAF, Cashman K (eds) The Cerro Galan Ignimbrite and Caldera: characteristics and origins of a very large volume ignimbrite and its magma system. Bull Volcanol. doi:10.1007/s00445-010-0410-7

Kent DV, Ninkovich D, Pescatore T, Sparks RSJ (1981) Paleomagnetic determination of emplacement temperature of Vesuvius A. D. 79 pyroclastic deposits. Nature 290:393–396

Lowrie W (1990) Identification of ferromagnetic minerals in a rock by coercivity and unblocking temperature properties. Geophys Res Lett 17(2):159–162

Mandeville CW, Carey S, Sigurdsson H, King J (1994) Paleomagnetic evidence for high-temperature emplacement of the 1883 subaqueous pyroclastic flows from Krakatau Volcano, Indonesia. J Geophys Res 99:9487–9504

Martì J, Diez-Gil JL, Ortiz R (1991) Conduction model for the thermal influence of lithic clasts in mixtures of hot gases and ejecta, J Geophys Res 96:21,879–21,885

Mason BG, Pyle DM, Oppenheimer C (2004) The size and frequency of the largest eruption on Earth. Bull Volcanol 66:735–748. doi:10.1007/s00445-004-0355-9

McClelland-Brown EA (1982) Discrimination of TRM and CRM by blocking-temperature spectrum analysis. Phys Earth Planet Int 30:405–414

McClelland EA, Druitt TH (1989) Paleomagnetic estimates of emplacement temperatures of pyroclastic deposits on Santorini, Greece. Bull Volcanol 51:16–27

McClelland E, Wilson CJN, Bardot L (2004) Palaeotemperature determinations for the 1.8-ka Taupo ignimbrite, New Zealand, and implications for the emplacement history of a high-velocity pyroclastic flow. Bull Volcanol 66:492–513. doi:10.1007/s00445-003-0335-5

Paterson GA, Roberts AP, Mac Niocaill C, Muxworthy AR, Gurioli L, Viramonte JG, Navarro C (2010) Paleomagnetic determination of emplacement temperatures of pyroclastic deposits: an underutilised tool. Bull Volcanol. doi:10.1007/s00445-009-0324-4

Porreca M, Giordano G, Mattei M, Musacchio P (2006) Evidence of two Holocene phreatomagmatic eruptions at Stromboli volcano (Aeolian Islands) from paleomagnetic data. Geophys Res Lett 33: L21316. doi:10.1029/2006GL027575

Porreca M, Mattei M, MacNiocaill C, Giordano G, McClelland E, Funiciello R (2008) Paleomagnetic evidence for low-temperature emplacement of the phreatomagmatic Peperino Albano ignimbrite (Colli Albani Volcano, Central Italy). Bull Volcanol 70:877–893. doi:10.1007/s00445-007-0176-8

Pullaiah GE, Irving E, Buchan KL, Dunlop DJ (1975) Magnetization changes caused by burial and uplift. Earth Planet Sci Lett 28:133–143

Quane SL, Russel K (2005) Ranking welding intensities in pyroclastic deposits. Bull Volcanol 67(2):129–143. doi:10.1007/s00445-004-0367-5

Riller U, Petrinovic I, Ramelow J, Strecker M, Oncken O (2001) Late Cenozoic tectonism, collapse caldera and plateau formation in the central Andes. Earth Planet Sci Lett 188:299–311

Salfity JA, Gorustovih S, Moya M, Amengual R (1984) Marco tectónico de la sedimentación y efusividad cenozoicas de la Puna Argentina. In: IX Congreso Geológico Argentino, Actas I, pp 5–515

Scott AC, Sparks RSJ, Bull ID, Knicker H, Evershed RP (2008) Temperature proxy data and their significance for the understanding of pyroclastic density currents. Geology 36(2):143–146. doi:10.1130/G24439A

Sparks RSJ, Francis PW, Hamer RD, Pankhurst RJ, O'Callaghan LO, Thorpe RS, Page R (1985) Ignimbrites of the Cerro Galán caldera, NW Argentina. J Volcanol Geotherm Res 24:205–248

Sulpizio R, Zanella E, Macìas JL (2008) Deposition temperature of some PDC deposits from the 1982 eruption of El Chichon volcano (Chiapas, Mexico) inferred from rock-magnetic data. J Volcanol Geotherm Res 175:494–500

Todesco M, Neri A, Esposti Ongaro T, Papale P, Rosi M (2006) Pyroclastic flow dynamics and hazard in a caldera setting: application to Phlegrean Fields (Italy). Geochem Geophys Geosys 7:11. doi:10.1029/2006GC001314

Viramonte JG, Galliski MA, Araña Saavedra V, Aparicio A, García Cacho L, C. Martín Escorza (1984) IX Congreso Geológico Argentino, Actas III, pp 234–254

Weaver R, Roberts AP, Barker AJ (2002) A late diagenetic (syn-folding) magnetization carried by pyrrhotite: implications for paleomagnetic studies from magnetic iron sulphide-bearing sediments. Earth Planet Sci Lett 200:371–386

Wright HMN, Lesti C, Cas RAF, Porreca M, Viramonte JG, Folkes CB, Giordano G (2011a) Columnar jointing in vapor phase altered, non-welded Cerro Galan Ignimbrite, Paycuqui, Argentina. In: Cas RAF, Cashman K (eds) The Cerro Galan Ignimbrite and Caldera: characteristics and origins of a very large volume ignimbrite and its magma system. Bull Volcanol. doi:10.1007/s00445-011-0524-6

Wright HMN, Folkes CB, Cas RAF, Cashman KV (2011b) Heterogeneous pumice populations in the 2.08 Ma Cerro Galán ignimbrite: implications for magma recharge and ascent preceding a large volume silicic eruption. In: Cas RAF, Cashman K (eds) The Cerro Galan Ignimbrite and Caldera: characteristics and origins of a very large volume ignimbrite and its magma system. Bull Volcanol. doi:10.1007/s00445-011-0525-5

Wright JV (1978) Remanent magnetism of poorly sorted deposits from the Minoan eruption of Santorini. Bull Volcanol 41:131–135

Zanella E, Gurioli L, Pareschi MT, Lanza R (2007) Influences of urban fabric on pyroclastic density currents at Pompeii (Italy): 2. Temperature of the deposits and hazard implications. J Geophys Res 112:B05214. doi:10.1029/2006JB004775

Zijderveld JDA (1967) Analysis of results. In: Collinson DW, Creer KM, Runcorn SK (eds) Methods in paleomagnetism. Elsevier, Amsterdam, pp 254–286

Zlotnicki J, Pozzi JP, Boudon G, Moreau MG (1984) A new method for the determination of the setting temperature of pyroclastic deposits (example Guadeloupe: French West Indies). J Volcanol Geotherm Res 21:297–312